Fourier's law and phonon localization in disordered harmonic crystals

Abhishek Chaudhuri[1,2], Anupam Kundu[1], Dibyendu Roy[1,3], Abhishek Dhar [1]

[1]*Raman Research Institute, C.V. Raman Avenue, Bangalore 560080, India*

[2]*Indian Institute of Science, Bangalore 560012, India and*

[3]*Weizmann Institute of Science, Rehovot 76100, Israel*

(Dated: February 6, 2020)

Abstract

We investigate the system size dependence of the heat current in two and three dimensional disordered harmonic lattices connected to stochastic white noise heat baths at different temperatures. The heat current is evaluated by numerical evaluation of the exact formula for current given in terms of the phonon transmission function, as well as by direct nonequilibrium simulations. We find that in the absence of an external potential, the conductivity, κ, has a power-law divergence with system size. In two dimensions, the associated exponent α depends on boundary conditions, while in three dimensions, it appears to be independent of boundary conditions. In the presence of a substrate potential at all sites of the crystal, the low frequency ballistic modes get cut off and one then expects transport to be strongly dominated by localization physics. In two dimensions we find exponential decay of κ with length for any disorder. In three dimensions, we find diffusive transport and hence validity of Fourier's law. We do not see a transition to an insulating phase with increasing disorder. A simple theory using ideas from both localization theory as well as kinetic theory is used to estimate the system size dependence of current and these are compared with the numerical results. We argue that the disagreement between the theoretical and numerical results points to the presence of anomalous phonon modes which cannot be classified either as localized, or diffusive, or as ballistic states.

PACS numbers:

I. INTRODUCTION

It is now about 200 years since Fourier proposed the famous law of heat conduction, a phenomenological law that states that for a macroscopic system the heat current density in a solid is proportional to the gradient in temperature. The constant of proportionality defines the thermal conductivity κ of the system and is expected to be an intrinsic material property of the system. A large amount of work over the past few decades have attempted to understand Fourier's law from a microscopic viewpoint. The surprising conclusion that has emerged is that this law is probably not valid for one and two dimensional systems except for the case when the system is in the presence of an external substrate potential [1, 2, 3]. Generically it is found that the heat current density J scales with system size N as

$$J \sim \frac{1}{N^\mu} \tag{1}$$

and hence effectively the thermal conductivity diverges as $\kappa \sim N^\alpha$ with $\alpha = 1 - \mu$. Recent experiments on heat conduction in nanotubes have reported observations which indicate divergence of κ with system size [4].

The general expectation is that Fourier's law should be valid in three dimensional solids in the presence of impurity scattering and phonon-phonon scattering of the Umpklapp type. There have been few simulational studies of heat conduction in three dimensional systems and so far none have been able to verify the validity of Fourier's law [5, 6]. In this paper we report extensive numerical and simulational studies of heat conduction in isotopically disordered harmonic crystals in two and three dimensions.

It is expected that the physics of heat conduction in disordered harmonic crystals should be affected by localization phenomena. Anderson localization is one of the most important features of disordered systems [7]. It is basically a feature characteristic of linear waves in disordered media, and has been most vigorously studied in the context of non-interacting electrons moving in a disordered potential. The physics of localization of electrons can be studied using two related approaches. One could look at the eigenstates and eigenfunctions of the isolated system of an electron in a disordered potential, and here one finds that in contrast to the spatially extended Bloch states in periodic potentials, there are now many eigenfunctions which are exponentially localized in space. Alternatively one can connect the system to leads at different chemical potentials and look at transport of electrons through the disordered system. In the linear response regime, this is equivalent to looking at the

transmission of electrons through the system at energies near the Fermi level. The transmission becomes drastically reduced when the state at the Fermi-level is localized. Among the few exact results, it has been shown by Mott and Twose and by Borland that in one dimension all states are exponentially localized [8]. In two dimensions there is no exact proof but it is believed that again all states are exponentially localized. In three and higher dimensions there is a transition from localized to extended states with increasing energy [9].

The physics of phonon localization is closely related to the electron localization problem. However there are two important differences. First, in the case of electronic transport, only states close to the Fermi level contribute (at the low temperatures one is usually interested in). On the other hand, for heat transport in a disordered crystal, the contribution of phonons of all frequencies have to be considered. The second difference is that low frequency phonon modes are weakly affected by disorder and always remain extended. We will see that these differences show up in transport properties. Again, as in the electronic case, the effect of localization is strongest in one dimension $(1D)$ where almost all modes are localized. The current carried by a mode which is localized on a length scale ℓ, falls with system size N as $e^{-N/\ell}$. Low frequency modes ($\omega \overset{<}{\sim} 1/N^{1/2}$ in $1D$) however are still extended and they are the main carriers of the heat current. The net current then depends on the population of these low frequency modes in the heat baths and their scattering due to boundary conditions (BCs). The observed system size dependence of κ in a one dimensional disordered harmonic chain can be understood completely from this picture [10, 11, 12, 13, 14, 15]. The main conclusions here are: (i) In the absence of a substrate potential, the conductivity has a power law dependence with system size, $i.e$ $\kappa \sim N^{\alpha}$. In the presence of a substrate the conductivity decays exponentially with system size. (ii) The exponent α depends on boundary conditions (BCs) and the spectral properties of the heat reservoirs. For white noise Langevin baths, one gets $\alpha = -1/2$ for fixed BC and $\alpha = 1/2$ for free BC.

Let us briefly review some of the known results for heat conduction in higher dimensional disordered harmonic systems.

Localization theory: A renormalization group study of phonon localization in a continuum scalar model was studied by John *et al.*[16]. They find that much of the predictions of the scaling theory of localization for electrons carry over to the phonon case. Specifically they predict: in $1D$ all modes with $\omega > 1/N^{1/2}$ are localized; in $2D$ all modes with $\omega > [\log(N)]^{-1/2}$ are localized; in $3D$ there is a finite band of frequencies of extended states.

However this study is not able to make any statements on the system size dependence of the conductivity.

Kinetic theory: For weak disorder and in dimensions $d > 1$, one might expect that localization effects can be neglected and then kinetic theory should be able to provide an accurate description. In this case one can think of Rayleigh scattering of phonons and this gives a mean free path $\ell_K(\omega) \sim 1/\omega^{d+1}$, for dimensions $d > 1$, and a diffusion constant $D(\omega) = v\ell_K(\omega)$ where v, the sound velocity can be taken to be a constant. For a finite system of linear dimension N we have $D(\omega) = vN$ for $\omega \lesssim N^{-1/(d+1)}$. Kinetic theory then gives [17]

$$
\begin{aligned}
\kappa &= \int_{N^{-1}}^{\infty} d\omega \rho(\omega) D(\omega) \\
&= \int_{N^{-1}}^{N^{-1/(d+1)}} d\omega \rho(\omega) vN + \int_{N^{-1/(d+1)}}^{\infty} d\omega \rho(\omega) v\ell_K(\omega) ,
\end{aligned}
$$

where the density of states $\rho(\omega) \sim \omega^{d-1}$ and we get $\kappa \sim N^{1/(d+1)}$.

Simulations: A disordered harmonic model in $2D$ was studied in simulations by Yang [18] who claimed that beyond some critical disorder one gets Fourier's law, *i.e* $\mu = 1$. However this result is probably incorrect. The simulations were done with Nose-Hoover heat baths and it is known that these can be problematic when applied to harmonic systems. Later simulations by Hu et al [19] on the same model but with stochastic heat baths do not find a Fourier behaviour. Lee and Dhar [20] studied the mass disordered $2D$ harmonic crystal with two different models of heat baths. Considering system size up to 256×256, with white noise baths they obtained $\mu \approx 0.59$ while with exponentially correlated noise they got $\mu \approx 0.51$.

Finally we note that recently experiments on heat conduction in isotopically disordered nanotubes have been performed [21] and there have been some theoretical analysis using Green's function methods in [22, 23].

In this paper we report results of heat conduction studies in disordered harmonic lattices with scalar displacements and connected to heat baths modeled by Langevin equations. We use two different approaches to study the nonequilibrium state. The first is a numerical one which relies on the result that the steady state current can be written exactly as an integral over a phonon transmission coefficient. This transmission coefficient can be written in terms of phonon Green's functions and we implement efficient numerical schemes to evaluate this.

The second approach is through direct nonequilibrium simulations of the Langevin equations of motion and finding the steady state current and temperature profiles. We also do studies of inverse participation ratios (IPR) of the normal modes of the isolated systems and correlate these with the results from the transmission study.

In order to see whether the strong dependence on boundary conditions observed in $1D$ is also present in higher dimensions, we have studied lattices with both fixed and free BCs. At first sight free BCs may appear somewhat unphysical in that the ends of the system are not held fixed. However the phonon transmission properties at low frequencies (which are most important) for this case is similar to those obtained for another model of bath, the so-called Rubin model. In the Rubin model (generalized to arbitrary dimensions) one connects the system to two semi-infinite ordered harmonic lattices each with the same structure as the system itself and at two different temperatures. In one dimension this model of bath is then exactly the same as the ideal leads used in the Landauer transport formalism. Thus both boundary conditions studied here are physically meaningful. Since low frequency modes can be suppressed in the presence of an external substrate potential, one expects qualitative differences in transport properties. We have thus considered both the cases with and without external pinning potentials.

We also propose heuristic arguments, based on localization theory and kinetic theory results, to estimate the system size dependence of current in various cases. The main idea behind our arguments is that the phonon states can be classified as ballistic modes, diffusive modes and localized modes. For the unpinned case (*i.e* in the absence of a substrate) we find disagreement between the theory and numerical results. We argue that this indicates the presence of anomalous states which are possibly super-diffusive. In the pinned case we find that in the two dimensional case we have a heat insulator while in three dimensions Fourier's law is valid and we have a normal conductor.

The paper is organized as follows. In Sec. (II) we present some general results for heat conduction in harmonic Hamiltonian systems connected to oscillator baths. We give the results of the Green's function and transfer matrix approaches. In Sec. (III) we define the specific model studied by us and some details of the numerical and simulational methods used in the paper. A brief review of results for the one dimensional case and the heuristic arguments for the higher dimensional cases are given in Sec. (IV). In Sec. (V) we present results from both the numerical approach as well as from nonequilibrium simulations. The

main results presented are for transmission functions, IPRs of normal modes and the system size dependence of the current in two and three dimensional disordered harmonic lattices. Finally we conclude with a discussion in Sec. (VI).

II. GENERAL RESULTS FOR HEAT CONDUCTION IN HARMONIC LATTICES

For simplicity we here consider the simplest case where longitudinal and transverse vibration modes are decoupled and hence we can describe the displacement at each site by a scalar variable. Also we restrict our study to $d-$ dimensional hyper-cubic lattices. Let us denote the lattice points by the vector $\mathbf{n} = \{n_1, n_2, ...n_d\}$ with $n_\nu = 1, 2, ...N$ for $\nu = 1, 2, ...d$. The displacement of a particle at the lattice site $\mathbf{n}$ is given by $x_\mathbf{n}$ and the corresponding momenta by $p_\mathbf{n}$. In the harmonic approximation the system Hamiltonian is given by

$$H = \sum_\mathbf{n} \frac{p_\mathbf{n}^2}{2m_\mathbf{n}} + \sum_{\mathbf{n},\hat{\mathbf{e}}} \frac{k}{2}(u_\mathbf{n} - u_{\mathbf{n}+\hat{\mathbf{e}}})^2 + \frac{k_o}{2} \sum_\mathbf{n} u_\mathbf{n}^2 , \tag{2}$$

where $\hat{\mathbf{e}}$ refers to the $2d$ nearest neighbors of any site and we have included an external substrate harmonic potential with spring constant k_o. Let us denote by $\mathcal{X}$ a column vector with N^d elements consisting of the displacements at all lattice sites. Similarly let $\mathcal{P}$ represent the vector for momenta at all sites. Then we can write the above Hamiltonian in the compact form:

$$H = \frac{1}{2}\mathcal{P}^T\mathcal{M}\mathcal{P} + \frac{1}{2}\mathcal{X}^T\mathcal{V}\mathcal{X} , \tag{3}$$

which defines the diagonal mass matrix $\mathcal{M}$ and the force constant matrix $\mathcal{V}$. We couple all the particles at $n_1 = 1$ and $n_1 = N$ (say) to heat reservoirs, at temperatures T_L and T_R respectively, so that heat conduction takes place along the $\nu = 1$ direction. Each layer with constant n_1 consists of $N' = N^{d-1}$ particles. The heat baths are modeled by writing white noise Langevin equations of motion for the particles coupled to the baths. Driven by the reservoirs at two different temperatures, the system reaches a nonequilibrium steady state. Our interest here is in the steady state current in the system. Formally one can obtain an exact solution of the Langevin equations of motion and from that obtain the steady state current [12, 24]. The expression for the total heat current from left to right reservoir is given

by:

$$I = \frac{k_B \Delta T}{4\pi} \int_{-\infty}^{\infty} d\omega \mathcal{T}(\omega) \tag{4}$$

$$\text{where} \quad \mathcal{T}(\omega) = 4 \, Tr[\mathcal{I}_L(\omega)\mathcal{G}^+(\omega)\mathcal{I}_R(\omega)\mathcal{G}^-(\omega)] \, ,$$

$$\text{and} \quad \mathcal{G}^+(\omega) = [-\omega^2 \mathcal{M} + \mathcal{V} - \mathcal{S}_L^+ - \mathcal{S}_R^+]^{-1} \, ,$$

where $\Delta T = T_L - T_R$, while $\mathcal{S}_L^+$, $\mathcal{S}_R^+$ are self-energy corrections coming from the left and right baths respectively, and $\mathcal{I}_{L,R} = Im[\mathcal{S}_{L,R}^+]$. The detailed forms of $\mathcal{S}_{L,R}^+$ depend on the properties of the reservoir and also on the coupling matrix between system and reservoirs. The matrix $\mathcal{G}^+(\omega)$ is the phonon Green's function of the system with self-energy corrections due to the baths. The term $\mathcal{T}(\omega)$ is effectively the transmission coefficient of phonons at frequency ω from left to right reservoir.

The above expression is of the Landauer form and has been derived using various other approaches such as scattering theory [25, 26] and the nonequilibrium Green's function formalism [27, 28]. In the case of electron transport through a disordered system, one would again get similar expressions but one would have to insert into Eq. (4) appropriate Fermi-distribution functions corresponding to the two reservoirs, and in the linear response regime one would get the Landauer expression for conductance $g = J_{el}/\Delta V = (e^2/\hbar)\mathcal{T}(E_F)$. We see that formally transport in both the disordered harmonic system and the electronic system are similar in that both are determined by transmission properties of noninteracting modes. The Green's function occurring in the formula for $\mathcal{T}$ is of course different for the two cases. As far as properties of eigenstates of the closed system is concerned, an exact mapping can be made between a tight-binding electron model with hopping elements t_{ij} and on-site potentials ϵ_i and the harmonic crystal Hamiltonian. This is obtained by the simple identification $t_{ij} \to \mathcal{V}_{ij}/(m_i m_j)^{1/2}$ for $i \neq j$ and $\epsilon_i \to \mathcal{V}_{ii}/m_i$. Thus the mass disorder case corresponds to a correlated disorder in both t_{ij} and ϵ_i.

We now outline steps by which $\mathcal{T}$ can be expressed in forms which are amenable to accurate numerical evaluation. Also we will give results whereby we express $\mathcal{T}$ in terms of product of random matrices. These are related to the Green's function and transfer matrix methods used earlier in the calculation of localization lengths in disordered electronic systems [29]. Some related discussions for the phonon case can be found in Refn .[30]. For heat conduction in one dimensional disordered chains, the transfer matrix approach has been shown to be very useful in obtaining analytic as well as accurate numerical results and here

we study the extension of this to higher dimensions.

Let us define the frequency $\Omega = (k/\bar{m})^{1/2}$, where $\bar{m}$ is the average mass. Then we can rewrite the formula Eq. (4) to get the current density in the following dimensionless form:

$$\mathcal{J} = \frac{I}{N' \, k_B \Delta T \Omega} = \frac{1}{4\pi N'} \int_{-\infty}^{\infty} d\omega \mathcal{T}(\omega) \tag{5}$$

where $\mathcal{T}$ has the same form as in Eq. (4) and we have now transformed to dimensionless variables $\omega \to \omega/\Omega, \mathcal{M} \to \mathcal{M}/\bar{m}, \mathcal{V} \to \mathcal{V}/k, \mathcal{S}_{L,R}^+ \to \mathcal{S}_{L,R}^+/k$. Recall that we are considering heat conduction in the $\nu = 1$ direction of a $d-$dimensional lattice with particles on the layers $n_1 = 1$ and $n_1 = N$ being connected to heat baths at temperatures T_L and T_R respectively. The matrices $\mathcal{S}_{L,R}^+$ and $\mathcal{Y} = -\mathcal{M}\omega^2 + \mathcal{V} - \mathcal{S}_L^+ - \mathcal{S}_R^+$ can then be written as $N \times N$ block matrices where each block is a $N' \times N'$ matrix. The block structures are as follows:

$$\mathcal{S}_L^+ = \begin{pmatrix} \Sigma_L^+ & 0 & \dots & 0 \\ 0 & 0 & \dots & 0 \\ 0 & 0 & \dots & 0 \\ 0 & 0 & \dots & 0 \end{pmatrix} \qquad \mathcal{S}_R^+ = \begin{pmatrix} 0 & 0 & \dots & 0 \\ 0 & 0 & \dots & 0 \\ 0 & 0 & \dots & 0 \\ 0 & 0 & \dots & \Sigma_R^+ \end{pmatrix} \tag{6}$$

$$\mathcal{Y} = \begin{pmatrix} -M_1\omega^2 + \Phi - \Sigma_L^+ & -I & 0 & \dots & 0 & 0 \\ -I & -M_2\omega^2 + \Phi & -I & \dots & 0 & 0 \\ 0 & -I & -M_3\omega^2 + \Phi & \dots & 0 & 0 \\ \cdot & \cdot & \cdot & \cdot & \cdot & \cdot \\ \cdot & \cdot & \cdot & \cdot & \cdot & \cdot \\ \cdot & \cdot & \cdot & \cdot & \cdot & \cdot \\ \cdot & \cdot & \cdot & \cdot & \cdot & -I \\ 0 & 0 & 0 & \cdot & -I & -M_N\omega^2 + \Phi - \Sigma_R^+ \end{pmatrix} \cdot$$

Here M_n denotes the diagonal mass-matrix for the $n_1 = n$ layer and Φ is a force-constant matrix whose off-diagonal terms correspond to coupling to sites within a layer. I is unit matrix and represents coupling between layers while 0 represents a matrix with all elements equal to zero. All these are $N' \times N'$ matrices. Finally Σ_L^+ and Σ_R^+ are $N' \times N'$ matrices which represent the coupling between the layers $n_1 = 1$ and N to the heat baths.

Let us define $\Gamma_{L,R} = Im[\Sigma_{L,R}^+]$. With the above form of $\mathcal{S}_{L,R}^+$, we find that the expression

for the transmission coefficient reduces to the following form:

$$\mathcal{T}(\omega) = 4\,Tr[\Gamma_L(\omega)G^+_{1,N}(\omega)\Gamma_R(\omega)G^-_{N,1}(\omega)]\,, \tag{7}$$

where $G^+_{1,N}$ is the $(1,N)^{\text{th}}$ block element of $\mathcal{G} = \mathcal{Y}^{-1}$. We now show that this element satisfies a simple recursion equation.

We first introduce some notation. Let $\mathcal{Y}^{(l,l+n-1)}$ with $1 \leq n \leq N - l + 1$ denote a $n \times n$ tridiagonal block matrix whose diagonal entries are $a_l, a_{l+1}, ...a_{l+n-1}$, where each a_l is a $N' \times N'$ matrix. The off-diagonal entries are given by $-I$. For a block matrix $\mathcal{A}^{(l,m)}$, $\mathcal{A}^{(l,m)}_{(i,j)}$ will denote the block sub-matrix of $\mathcal{A}^{(l,m)}$ beginning with i^{th} block row and column and ending with the jth block row and column, while $A^{(l,m)}_{i,j}$ will denote the $(i,j)^{\text{th}}$ block element of $\mathcal{A}^{(l,m)}$. Also $\mathcal{I}_n$ will denote a $n \times n$ block-diagonal matrix with diagonal elements I.

With this notation the matrix $\mathcal{Y} = \mathcal{Y}^{(1,N)}$ has the following structure:

$$\mathcal{Y}^{(1,N)} = \begin{pmatrix} a_1 & -I & 0 & ... & 0 & 0 \\ -I & a_2 & -I & ... & 0 & 0 \\ 0 & -I & a_3 & ... & 0 & 0 \\ . & . & . & . & . & . \\ . & . & . & . & . & . \\ . & . & . & . & . & . \\ . & . & . & . & a_{N-1} & -I \\ 0 & 0 & 0 & . & -I & a_N \end{pmatrix} = \begin{pmatrix} \mathcal{Y}^{(1,N-1)} & \mathcal{W}_N \\ \mathcal{W}_N^T & a_N \end{pmatrix} \tag{8}$$

where $\mathcal{W}_N^T = (0,0,...,-I)$ is a $1 \times N - 1$ block vector. The inverse of $\mathcal{Y}^{(1,N)}$ is denoted by $[\mathcal{Y}^{(1,N)}]^{-1} = \mathcal{G}^{(1,N)}$ and satisfies the equation:

$$\mathcal{Y}^{(1,N)}\,\mathcal{G}^{(1,N)} = \mathcal{I}_N\,,$$

We now write the above equation in the form:

$$\begin{pmatrix} \mathcal{Y}^{(1,N-1)} & \mathcal{W}_N \\ \mathcal{W}_N^T & a_N \end{pmatrix} \begin{pmatrix} \mathcal{G}^{(1,N)}_{(1,N-1)} & \mathcal{U}_N \\ \mathcal{U}_N^T & G^{(1,N)}_{N,N} \end{pmatrix} = \begin{pmatrix} \mathcal{I}_{N-1} & 0 \\ 0 & I \end{pmatrix}\,, \tag{9}$$

where $\mathcal{U}_N^T = [G^{(1,N)T}_{1,N}, G^{(1,N)T}_{2,N}..., G^{(1,N)T}_{N-1,N}]$ is a $1 \times N - 1$ block vector. From Eq (9) we get

the following four equations

$$\mathcal{Y}^{(1,N-1)} \, \mathcal{G}^{(1,N)}_{(1,N-1)} + \mathcal{W}_N \, \mathcal{U}^T_N = \mathcal{I}_{N-1}$$

$$\mathcal{W}^T_N \, \mathcal{G}^{(1,N)}_{(1,N-1)} + a_N \, \mathcal{U}^T_N = 0$$

$$\mathcal{Y}^{(1,N-1)} \, \mathcal{U}_N + \mathcal{W}_N \, G^{(1,N)}_{N,N} = 0$$

$$\mathcal{W}^T_N \, \mathcal{U}_N + a_N \, G^{(1,N)}_{N,N} = I \qquad (10)$$

Noting that $[\mathcal{Y}^{(1,N-1)}]^{-1} = \mathcal{G}^{(1,N-1)}$ we get, using the third equation above and the form of $\mathcal{W}_N$:

$$\mathcal{U}_N = -\mathcal{G}^{(1,N-1)}\mathcal{W}_N G^{(1,N)}_{N,N}$$

$$\text{or} \quad G^{(1,N)}_{i,N} = G^{(1,N-1)}_{i,N-1}G^{(1,N)}_{N,N} \quad \text{for} \quad i = 1,2...N-1 . \qquad (11)$$

From the fourth equation in Eq. (10) we get:

$$G^{(1,N)}_{N-1,N} = a_N \, G^{(1,N)}_{N,N} - I . \qquad (12)$$

We will now use Eqs. (11,12) to obtain a recursion for $G^{(1,N)}_{1,N}$ $[= G^+_{1,N}$ in Eq. (7)], which is the main object of interest. Let us define $P^{(l,n)} = [G^{(l,n)}_{1,n-l+1}]^{-1}$ where $\mathcal{G}^{(l,m)} = [\mathcal{Y}^{(l,m)}]^{-1}$. Then setting $i = 1$ in Eq. (11) and taking an inverse on both sides we get:

$$P^{(1,N)} = [G^{(1,N)}_{N,N}]^{-1} \, P^{(1,N-1)}. \qquad (13)$$

Setting $i = N-1$ in Eq. (11) we get $G^{(1,N)}_{N-1,N} = G^{(1,N-1)}_{N-1,N-1}G^{(1,N)}_{N,N}$ and using this in Eq. (12) we get $[G^{(1,N)}_{N,N}]^{-1} = [a_N - G^{(1,N-1)}_{N-1,N-1}]$. Inserting this in the above equation we finally get our required recursion relation:

$$P^{(1,N)} = a_N P^{(1,N-1)} - P^{(1,N-2)} . \qquad (14)$$

The initial conditions for this recursion are: $P^{(1,0)} = I_M$ and $P^{(1,1)} = a_1$. By proceeding similarly as before we can also obtain the following recursion relation:

$$P^{(n,N)} = P^{(n+1,N)}a_1 - P^{(n+2,N)} , \qquad (15)$$

and $P^{(1,N)}$ can be recursively obtained using the initial conditions $P^{(N+1,N)} = I_M$ and $P^{(N,N)} = a_N$. Given the set $\{a_i\}$, by iterating either of the above equations one can numerically find $P^{(1,N)}$ and then invert it to find $G^{(1,N)}_{1,N}$. However this scheme runs into accuracy

10

problems since the numerical values of the matrix elements of the iterates grow rapidly. We describe now a different way of performing the recursion which turns out to be numerically more efficient. We first define

$$r_N = P^{(1,N)}[P^{(1,N-1)}]^{-1} . \tag{16}$$

From Eq. (14) we immediately get:

$$r_N = a_N - \frac{1}{r_{N-1}} , \tag{17}$$

with the initial condition $r_1 = a_1$. Then $G_{1,N}^{(1,N)}$ is given by:

$$\begin{aligned} G_{1,N}^{(1,N)} &= [P^{(1,N)}]^{-1} = [r_N r_{N-1}...r_1]^{-1} \\ &= r_1^{-1} r_2^{-1}...r_N^{-1} . \end{aligned} \tag{18}$$

This form where at each stage r_l^{-1} is evaluated turns out to be numerically more accurate.

Finally we show that one can express $G_{1,N}^{(1,N)}$ in the form of a product of matrices. The product form is such that the system and reservoir contributions are separated. First we note that the form of the matrices a_l for our specific problem is:

$$a_l = c_l - \delta_{l,1}\Sigma_1 - \delta_{l,N}\Sigma_N \tag{19}$$

$$\text{where} \quad c_l = -M_l\omega^2 + \Phi .$$

Thus the forms of a_1 and a_N are different because of the extra terms coming from the coupling to reservoirs. We define system-dependent matrices $Q^{(1,n)}$, $Q^{(n,N)}$ by replacing a_1, a_N by c_1, c_N in the recursions for Ps'. Thus $Q^{(1,n)} = P^{(1,n)}(a_1 \to c_1, a_N \to c_N)$ and $Q^{(n,N)} = P^{(n,N)}(a_1 \to c_1, a_N \to c_N)$. Clearly Qs' satisfy the same recursion as the Ps' with a_l replaced by c_l. Then using Eqs. (14,15), and similar equations for the Qs' we get:

$$\begin{aligned} P^{(1,N)} &= Q^{(1,N)} - Q^{(2,N)} \Sigma_1 - \Sigma_N Q^{(1,N-1)} + \Sigma_N Q^{(2,N-1)} \Sigma_1 \\ &= (1 \quad -\Sigma_N) \begin{pmatrix} Q^{(1,N)} & -Q^{(2,N)} \\ Q^{(1,N-1)} & -Q^{(2,N-1)} \end{pmatrix} \begin{pmatrix} 1 \\ \Sigma_1 \end{pmatrix} \end{aligned} \tag{20}$$

From the recursion relations for the Qs' it is easy to see that:

$$\begin{aligned} \begin{pmatrix} Q^{(1,N)} & -Q^{(2,N)} \\ Q^{(1,N-1)} & -Q^{(2,N-1)} \end{pmatrix} &= \begin{pmatrix} a_N & -I \\ I & 0 \end{pmatrix} \begin{pmatrix} Q^{(1,N-1)} & -Q^{(2,N-1)} \\ Q^{(1,N-2)} & -Q^{(2,N-2)} \end{pmatrix} \\ &= \hat{T}_N \hat{T}_{N-1}...\hat{T}_1 \\ \text{where} \quad \hat{T}_l &= \begin{pmatrix} a_l & -I \\ I & 0 \end{pmatrix} \end{aligned} \tag{21}$$

11

III. MODELS AND METHODS

We consider the Hamiltonian in Eq. (2) with nearest neighbor harmonic interaction. The heat baths are modeled through Langevin equations with Gaussian white noise. We will use the notation $\mathbf{n} = (n_1, \mathbf{n'})$. The equations of motion are given by:

$$\mathcal{M}_\mathbf{n} \ddot{x}_\mathbf{n} = -\sum_\mathbf{k} \mathcal{V}_{\mathbf{n},\mathbf{k}} x_\mathbf{k} + \delta_{n_1,1}(-\gamma \dot{x}_{(1,\mathbf{n'})} + \eta^L_{\mathbf{n'}}) + \delta_{n_1,N}(-\gamma \dot{x}_{(N,\mathbf{n'})} + \eta^R_{\mathbf{n'}}) \tag{22}$$

where the dissipative and noise terms are related by the usual fluctuation dissipation relations

$$\langle \eta^L_{\mathbf{n'}}(t) \eta^L_{\mathbf{k'}}(t') \rangle = 2k_B T_L \delta(t - t') \delta_{\mathbf{n'k'}}$$
$$\langle \eta^R_{\mathbf{n'}}(t) \eta^R_{\mathbf{k'}}(t') \rangle = 2k_B T_R \delta(t - t') \delta_{\mathbf{n'k'}} \ . \tag{23}$$

We consider a binary mass disordered crystal. Specifically we set the masses of exactly half the particles at randomly chosen sites to be $1 - \Delta$ and the rest to $1 + \Delta$. Thus Δ gives a measure of the disorder. For the particles connected to baths we will study two kinds of boundary conditions, namely (i) fixed boundary conditions: $x_{(0,\mathbf{n'})} = x_{(N+1,\mathbf{n'})} = 0$ and (ii) free boundary conditions: $x_{(0,\mathbf{n'})} = x_{(1,\mathbf{n'})}$, $x_{(N,\mathbf{n'})} = x_{(N+1,\mathbf{n'})}$. Periodic boundary conditions are imposed in all other directions. Given the Langevin equations of motion Eq (22), we can at once find the corresponding self-energy corrections terms $\Sigma^+_{L,R}$. For the present case we have

$$\Sigma^+_{L,R} = \frac{i\gamma\omega}{\bar{m}\Omega} I \ . \tag{24}$$

Numerical approach: In our numerical calculations we use the above form of $\Sigma^+_{L,R}$. Then with $a_1 = -M_1\omega^2 + \Phi - \Sigma^+_L$, $a_N = -M_N\omega^2 + \Phi - \Sigma^+_R$ and $a_l = -M_l\omega^2 + \Phi$ for $l = 2, 3...N-1$, we use the recursion relations in Eq. (17,18) to evaluate the required Green's function. Computing the trace in Eq. (7) then gives us the transmission coefficient as a function of frequency. For the large system sizes we study, the transmission $\mathcal{T}(\omega)$ has appreciable values only within the range of frequencies of normal modes of the isolated system. By performing a discrete sum over the allowed range of frequencies we can perform the integration in Eq. (5) to obtain the heat current density J. In performing the discrete sum over ω step sizes of $\delta\omega = 0.01 - 0.0001$ were used and we verified convergence in most cases. The parameters $k = 1, \bar{m} = 1$ were kept fixed and different values of the mass variance Δ and the on-site spring constant k_o were studied for two and three dimensional lattices. It is expected that

the value of the exponent μ should not depend on γ and in all our calculations we mostly have $\gamma = 1$ except when otherwise specified.

Simulation approach: The simulations of Eq. (22) were performed using a velocity-verlet scheme as given in Refn. [31]. The current and temperature profiles in the system were obtained from the following time averages obtained in the nonequilibrium steady state:

$$
\mathcal{J}_n = -\frac{1}{N'} \sum_{\mathbf{n'}} k \langle\, [x_{(n-1,\mathbf{n'})} - x_{(n,\mathbf{n'})}]\, \dot{x}_{(n,\mathbf{n'})} \,\rangle \quad n = 2, 3, ...N
$$

$$
k_B T_n = \frac{1}{N'} \sum_{\mathbf{n'}} m_{(n,\mathbf{n'})} \langle\, \dot{x}^2_{(n,\mathbf{n'})} \,\rangle \quad n = 1, 2, ...N \ .
$$

In the steady state one has $\mathcal{J}_n = \mathcal{J}$ for all n and in the simulations equilibration can be verified by checking how accurately this is satisfied. We choose a step size of $\Delta t = 0.005$ and equilibrated the system for over 10^8 time steps and then current and temperature profiles were obtained by averaging over another 10^8 time steps. The parameters $T_L = 2.0, T_R = 1.0, k = 1, \gamma = 1, \bar{m} = 1$ were kept fixed and different values of the mass variance Δ and the on-site spring constant k_o were studied for two and three dimensional lattices of different sizes.

The value of $\mathcal{T}(\omega)$, $\mathcal{J}$ and T_n of course depend on the particular disorder realization. Mostly we will here be interested in disorder averages of these quantities which we will denote by $[\mathcal{T}], J = [\mathcal{J}]$ and $[T_n]$. We also define the disorder averaged transmission per bond with the notation

$$
T(\omega) = \frac{1}{N'}[\mathcal{T}(\omega)] \ .
$$

Numerical analysis of eigenmodes and eigenfunctions We have also studied the properties of the normal modes of the isolated disordered harmonic lattices, *i.e*, in the absence of coupling to reservoirs. The $d-$dimensional lattice has $p = 1, 2, ...N^d$ normal modes and we denote the displacement field corresponding to the pth mode by $a_{\mathbf{n}}(p)$ and the corresponding eigenvalue by $\epsilon_p = \omega_p^2$. The normal mode equation corresponding to the Hamiltonian in Eq. (2) is given by:

$$
m_{\mathbf{n}} \omega_p^2 a_{\mathbf{n}} = (2dk + k_o)a_{\mathbf{n}} - k \sum_{\hat{\mathbf{e}}} a_{\mathbf{n}+\hat{\mathbf{e}}} \ . \tag{25}
$$

Introducing variables $\psi_{\mathbf{n}}(p) = m_{\mathbf{n}}^{1/2} a_{\mathbf{n}}(p)$, $v_{\mathbf{n}} = (2dk + k_o)/m_{\mathbf{n}}$ and $t_{\mathbf{n},\mathbf{k}} = k/(m_{\mathbf{n}} m_{\mathbf{k}})^{1/2}$ for

nearest neighbour sites $\mathbf{n}$, $\mathbf{k}$ the above equation transforms to the following form:

$$\omega_p^2 \psi_{\mathbf{n}}(p) = v_{\mathbf{n}} \psi_{\mathbf{n}}(p) - \sum_{\mathbf{k}} t_{\mathbf{n},\mathbf{k}} \psi_{\mathbf{k}}(p) . \tag{26}$$

This has the usual structure of an eigenvalue equation corresponding to a tight-binding Hamiltonian with nearest neighbour hopping $t_{\mathbf{n},\mathbf{k}}$ and on-site energies $v_{\mathbf{n}}$. We have numerically evaluated all eigenvalues and eigenstates of the above equation for small lattices. One measure of the degree of localization of a given mode is the inverse participation ratio (IPR) defined as follows:

$$P^{-1} = \frac{\sum_{\mathbf{n}} a_{\mathbf{n}}^4}{(\sum_{\mathbf{n}} a_{\mathbf{n}}^2)^2} . \tag{27}$$

For a completely localized state it takes the value 1 while for a completely delocalized state it takes the value $1/N^d$. We will present numerical results for the participation ratio calculated for all eigenstates of given disorder realizations, in both $2D$ and $3D$.

IV. RESULTS IN $1D$ AND HEURISTIC ARGUMENTS FOR HIGHER DIMENSIONS

Heat conduction in the one dimensional disordered harmonic chain has been extensively studied and is more or less well understood [10, 11, 12, 13, 14, 15]. The matrix formulation explained in the last section leads to a clear analytic understanding of the main results. The current is given by the general expression Eq. (5) but now the transmission is given by $\mathcal{T}(\omega) = 4\gamma^2 \omega^2 |G_{(1,N)}|^2$ where $G_{(1,N)}$ is now just a complex number. The disordered averaged transmission is given by $T(\omega) = [\mathcal{T}(\omega)]$. There are three observations that enable one to determine the asymptotic system size dependence of current. These are:

(i) we note that $P^{(1,N)} = [G_{1,N}^+]^{-1}$ given by Eqs. (20,21) is a complex number which can be expressed in terms of the product of N random 2×2 matrices. Using results from the theory of product of random matrices it can be shown that for almost any disorder realization, $|P^{(1,N)}| \sim e^{bN\omega^2}$ where b is a constant. Since $\mathcal{T}(\omega) \sim |P^{(1,N)}|^{-2}$ this implies that transmission is significant only for low frequencies $\omega \overset{<}{\sim} \omega_c \sim 1/N^{1/2}$. Thus one needs to look at the small ω behaviour of $T(\omega)$.

(ii) The second observation made in Refn. [14] is that transmission for $\omega < \omega_c$ is ballistic in the sense that $T(\omega)$ is insensitive to the disorder.

(iii) The final important observation is that the form of $T(\omega)$ at small ω depends strongly on boundary conditions and bath properties [14, 15]. For the white noise Langevin baths one finds $T(\omega) \sim \omega^2$ for fixed BC and $T(\omega) \sim \omega^0$ for free BC [15]. This difference basically arises because of scattering of long wavelength modes by the boundary pinning potentials.

In Fig. (1) we plot $T(\omega)$ for the $1D$ binary mass-disordered lattice with both fixed and free boundary conditions. One can clearly see the two features discussed above namely (i) dependence of frequency cut-off on system size and (ii) dependence of form of $T(\omega)$ on boundary conditions. Using the three observations made above it is easy to arrive at the conclusion that $J \sim N^{-3/2}$ for fixed BC and $J \sim N^{-1/2}$ for free BC. In the presence of a pinning potential at all sites, the low-frequency modes get suppressed and then one gets a heat insulator with $J \sim e^{-aN}$ [32].

Higher dimension: Let us try to extend the analysis of the $1D$ case to higher dimensions. For this we will also use inputs from both kinetic theory and the theory of phonon localization. Corresponding to the three observations made above for the $1D$ case we now make the following arguments:

(i) From localization theory one expects all finite-frequency states in a $2D$ disordered system to be localized. In $3D$ we expect finite frequency states to be either localized or extended (*and diffusive*).

(ii) For the unpinned case there will exist low frequency states, in both $2D$ and $3D$, which will be ballistic in the sense that they are insensitive to the disorder and the transmission coefficient at these frequencies will be almost the same as for the ordered case. To find the frequency cut-off below which states are ballistic we use kinetic theory results. For the low-frequency extended states we expect kinetic theory to be reliable and this gives us a mean free path for phonons $\ell_K \sim \omega^{-(d+1)}$. This means that for low frequencies $\omega \stackrel{<}{\sim} N^{-1/(d+1)}$ we have $\ell_K(\omega) > N$ and phonons transmit ballistically. We now proceed to calculate the contribution of these ballistic modes to the total current. This can be obtained by looking at the small ω form of $T(\omega)$ for the ordered lattice.

(iii) For the ordered lattice $T(\omega)$ is typically a highly oscillatory function with the oscillations increasing with system size. An effective transmission coefficient in the $N \to \infty$ limit can be obtained by considering the integrated transmission. This asymptotic *effective* low-frequency form of $T(\omega)$, for the ordered lattice can be calculated using methods described

in Refn. [15] and is given by [33]:

$$T(\omega) \sim \omega^{d+1} \quad \text{for fixed BC}$$

$$T(\omega) \sim \omega^{d-1} \quad \text{for free BC} ,$$

the result being valid for $d = 1, 2, 3$.

Using the above arguments we then get the ballistic contribution to the total current density (for unpinned case) as:

$$J_{\text{ball}} \sim \int_0^{N^{-1/(d+1)}} d\omega \, \omega^{d+1} \sim \frac{1}{N^{(d+2)/(d+1)}} \quad \text{fixed BC,}$$

$$\sim \int_0^{N^{-1/(d+1)}} d\omega \, \omega^{d-1} \sim \frac{1}{N^{d/(d+1)}} \quad \text{free BC.} \quad (28)$$

We can now make predictions for the asymptotic system size dependence of total current density in two and three dimensions.

Two dimension: From localization theory one knows that all finite frequency modes $\omega > (\ln N)^{-1/2}$ are localized and their contribution to total current falls exponentially with system size. Based on a kinetic theory picture let us assume that the low frequency extended states are either diffusive (for $N^{-1/3} < \omega < (\ln N)^{-1/2}$) or ballistic (for $\omega < N^{-1/3}$). The diffusive contribution to total current will then scale as $J_{\text{diff}} \sim (\ln N)^{-1/2} N^{-1}$. The ballistic contribution depends on BCs and is given by Eq. (28). This gives $J_{\text{ball}} \sim N^{-4/3}$ for fixed BC and $J_{\text{ball}} \sim N^{-2/3}$ for free BC. Hence, adding all the different contributions, we conclude that asymptotically:

$$J \sim \frac{1}{(\ln N)^{1/2} N} \quad \text{fixed BC,}$$

$$\sim \frac{1}{N^{2/3}} \quad \text{free BC.} \quad (29)$$

In the presence of an onsite pinning potential at all sites the low frequency modes get cut off and since all the remaining states are localized, hence we expect:

$$J \sim e^{-bN}, \quad \text{pinned} \quad (30)$$

where b is a constant.

Three dimension: In this case localization theory tells us that at finite frequencies there are bands of localized as well as extended states. Assuming that the extended states are

all diffusive, the contribution from finite frequency modes thus scales as $J_{\text{diff}} \sim N^{-1}$. The ballistic contribution (from states with $\omega < N^{-1/4}$) is obtained from Eq. (28) and gives $J_{\text{ball}} \sim N^{-5/4}$ for fixed BC and $J_{\text{ball}} \sim N^{-3/4}$ for free BC. Hence, adding all contributions, we conclude that asymptotically:

$$
\begin{aligned}
J &\sim \frac{1}{N} && \text{fixed BC,} \\
&\sim \frac{1}{N^{3/4}} && \text{free BC.}
\end{aligned}
\tag{31}
$$

In the presence of an onsite pinning potential at all sites the low frequency modes get cut off and since in this case the remaining states form bands of diffusive and localized states, hence we expect:

$$
J \sim \frac{1}{N} \qquad \text{pinned.}
\tag{32}
$$

Thus in $3D$ both the unpinned lattice with fixed boundary conditions and the pinned lattice are expected to show Fourier type of behaviour as far as the system size dependence of current is considered.

Note that for free BC, the prediction for the current contribution from the ballistic part $J_{\text{ball}} \sim N^{-d/(d+1)}$ is identical to that from kinetic theory discussed in Sec. (I). This agreement can be traced to the small ω form of $T(\omega) \sim \omega^{d-1}$ which is identical to the form of the density of states $\rho(\omega)$ used in kinetic theory. The typical form of density of states for disordered lattices is shown in Fig. (2) and we can see that the low frequency form is similar to the ordered case and has the expected ω^{d-1} behaviour. However it seems reasonable to expect that for the transport current phonons are being injected at the boundaries and so, in the kinetic theory, one needs to use the *local density of states* evaluated at the boundaries. For fixed BC this will then give rise to an extra factor of ω^2 (from the squared wavefunction) and then the kinetic theory prediction matches with those given above.

V.   RESULTS FROM NUMERICS AND SIMULATIONS

We now present the numerical and simulation results for transmission coefficients, heat current density, temperature profiles and IPRs for the disordered harmonic lattice in various dimensions. The numerical scheme for calculating J is both faster and more accurate than simulations. Especially, for strong disorder, equilibration times in simulations becomes very

large and in such cases only the numerical method can be used. However we have also shown some simulation results and their almost perfect agreement with the numerical results provides additional confidence on the accuracy of our results. In Sec. (V A) we give the results for the $2D$ lattice for the unpinned case with both fixed and free boundary conditions and then for the pinned case. In Sec. (V B) we present the results for the three dimensional case with and without substrate pinning potentials.

A. Results in two-dimensions

In this section we consider $N \times N$ square lattices with periodic BCs in the $\nu = 2$ direction and either fixed or free BCs in the conducting direction ($\nu = 1$). One of the interesting questions here is as to how the three observations for the $1D$ case discussed in Sec. (IV) get modified for the $2D$ case.

1. Disordered $2D$ lattice without a substrate potential

Fixed BC: we have computed the transmission coefficients and the corresponding heat currents for different values of Δ and for system sizes from $N = 16 - 1024$. The number of averages varied from over 100 samples for $N = 16$ to about one or two samples for $N = 1024$. In Figs. (3,4) we plot the disorder averaged transmission coefficient for two different disorder strengths, $\Delta = 0.2$ and $\Delta = 0.8$, for different system sizes. The corresponding plots of IPRs as a function of normal mode frequency ω_p, for single disorder realizations, are also given. From the IPR plots we get an idea of the typical range of allowed normal mode frequencies and their degree of localization. Low IPR values which scale as N^{-2} imply extended states while large IPR values which do not change much with system size denote localized states. In Fig. (4) we also show typical plots of small IPR and large IPR wavefunctions. From Figs. (3,4) we make the following observations:

(i) As expected we see significant transmission only over the range of frequencies with extended states. Thus for $\Delta = 0.2$ we see that for the largest system studied ($N = 512$), transmission is appreciable in the range $\omega \approx (0 - 2)$ and this is also roughly the range where the IPR data shows a N^{-2} scaling behaviour. For $\Delta = 0.8$ the full range of normal modes is $\omega_p \approx (0 - 6)$ with a gap around $\omega_p \approx (2 - 2.2)$. However the IPR plot shows that only

states in the range $\omega_p \approx (0 - 1.5)$ are extended and correspondingly we see transmission mostly in this range. Unlike the $1D$ case we do not see any significant dependence on system size of the upper frequency cut-off ω_c beyond which states are localized and transmission is negligible. As discussed earlier, localization theory predicts $\omega_c \sim (\ln N)^{-1/2}$ and this may be difficult to observe numerically.

(ii) The overall transmission function $T(\omega)$ decreases with increasing system size but we have not been able to find any simple scaling behaviour. In Fig. (3) we have also plotted $T(\omega)$ for the ordered binary mass case and we note that over a range of small frequencies, $T(\omega)$ for the disordered case is very close to the curve for the ordered case, which means that these modes are ballistic. As expected from the arguments in Sec. (IV) we roughly find $T(\omega) \sim \omega^3$ at small frequencies. The nature of the remaining transmitting states is unclear. Both from the transmission and IPR plots they appear to be extended states. But they do not have a N^{-1} scaling and so are not diffusive. In fact they decrease much slower than N^{-1} with system size which indicates that they are super-diffusive states.

We next look at the the integrated transmission which gives the net heat current. The system size dependence of the disorder averaged current J for different values of Δ is shown in Fig. (5). For the case $\Delta = 0.2$, we also show simulation results and one can see that there is excellent agreement with the numerical results. For $\Delta = 0.2$ we get an exponent $\mu \approx 0.6$ which is close to the value obtained earlier in Refn. (20) for a similar disorder strength. However with increasing disorder we see that this value changes and seems to settle to around $\mu \approx 0.75$. It seems reasonable to expect (though we have no rigorous arguments) that there is only one asymptotic exponent and for small disorder one just needs to go to very large system sizes to see the true value. In Fig. (6) we show temperature profiles obtained from simulations for lattices of different sizes and with $\Delta = 0.2$. The jumps at the boundaries indicate that the asymptotic size limit has not yet been reached. This is consistent with our result that the exponent μ obtained at $\Delta = 0.2$ is different from what we believe is the correct asymptotic value (obtained at larger values of Δ). We do not have temperature plots at strong disorder where simulations are difficult.

Thus contrary to the arguments in Sec. (IV) which predicted $J \sim (\ln N)^{-1/2} N^{-1}$ we find a much larger current scaling as $J \sim N^{-0.75}$. From our studies of the transmission coefficient we have found the presence of extended states which appear to be super-diffusive and we believe that the presence of these states leads to a breakdown of the arguments given earlier.

Free BC: In this case from the arguments in Sec. (IV) we expect ballistic states to contribute most significantly to the current density giving $J_{\mathrm{ball}} \sim N^{-2/3}$. The super-diffusive states are presumably unaffected by boundary conditions and, from the results for fixed BC, we expect their contribution to current to scale as $N^{-0.75}$. Hence the overall current should scale in the asymptotic limit as $J \sim N^{-2/3}$.

In Figs. (7,8) we plot the disorder averaged transmission coefficient for $\Delta = 0.2$ and $\Delta = 0.8$ for different system sizes. Qualitatively these results look very similar to those for fixed boundaries. However transmission is now significantly larger in the region of extended states. The behaviour at frequencies $\omega \to 0$ is also different and we now find $T(\omega) \sim \omega$ in contrast to $T(\omega) \sim \omega^3$ for fixed boundaries. From the plots of IPRs in Fig. (8) we note that there is not much qualitative difference with the fixed boundary plots.

The system size dependence of the disorder averaged current J for two different values of Δ is shown in Fig. (9). For $\Delta = 0.2$ we get an exponent $\mu \approx 0.5$ while for the stronger disorder case we see a different exponent $\mu \approx 0.6$. Again we believe that the strong disorder value of $\mu = 0.6$ is closer to the value of the true asymptotic exponent. This value is close to the expected $\mu = 2/3$ for free BC and significantly different from the value obtained for fixed BC ($\mu \approx 0.75$). Thus the dependence of the value of σ on boundary conditions exists even in the $2D$ case.

2. *Disordered $2D$ lattice with a substrate potential*

We now study the effect of introducing a harmonic pinning potential at all sites of the lattice. It is expected that this will cut off low frequency modes and hence one should see strong localization effects. The localization length ℓ should decrease both with increasing Δ and increasing k_o [in $1D$ heuristic arguments give $\ell \sim 1/(\Delta^2 k_o)$]. In Figs. (10,11) we plot the transmission coefficients for two cases with on-site potentials $k_o = 10.0$ and $k_o = 2.0$ respectively, and $\Delta = 0.4$. We also plot the IPR in Fig. (10). Unlike in the unpinned case we now find that the transmission coefficients are much smaller and fall more rapidly with system size.

From the plot of P^{-1} we find that for all the modes, the value of P^{-1} does not change much with system size and thus in this case all states are localized. The allowed frequency bands correspond to the transmission bands. The two wavefunctions plotted in Fig. (10)

correspond to small and large P^{-1} values and clearly show that both states are localized.

The system size dependence of the integrated current is shown in Fig. (12) for the two parameter sets. The values of $\mu \approx 1.6, 3.65$ for the two sets indicate that at large enough length scales one will get a current falling exponentially with system size and hence we have an insulating phase. In Fig. (13) we plot the temperature profiles for the set with $\Delta = 0.4, k_o = 10.0$. In this case it is difficult to obtain steady state temperature profiles from simulations for larger system sizes. The reason is that the temperature (unlike current) gets equal contributions from all modes (both localized and extended) and equilibrating the localized modes takes a long time.

B.   Results in three-dimensions

In this section we mostly consider $N \times N \times N$ lattices with periodic boundary conditions in the $\nu = 2, 3$ directions and both fixed and free boundary conditions in the conducting direction ($\nu = 1$). Some results for $N \times N_2 \times N_3$ lattices with $N_2 = N_3 < N$ will also be discussed. Preliminary results for the case of free BCs are given and indicate that there is no dependence of the exponent σ on BCs.

1.   Disordered 3D lattice without a substrate potential

Fixed BC: we have used both the numerical approach and simulations for sizes up to $32 \times 32 \times 32$ for which we have data for $T(\omega)$. For larger systems the matrices become too big and we have not been able to use the numerical approach. Hence, for larger system sizes we have only performed simulations, including some on $N \times N_2 \times N_2$ lattices. For these cases only the current J is obtained. The number of averages varied from over 100 samples for $N = 16$ to two samples for $N = 64$. In Figs. (14,15) we plot the disorder averaged transmission coefficient for two different disorder strengths, $\Delta = 0.2$ and $\Delta = 0.8$, for different system sizes. The corresponding plots of IPRs as a function of normal mode frequency ω_p, for single disorder realizations, are also given. From the IPR plots we get an idea of the typical range of allowed normal mode frequencies and their degree of localization. Low IPR values which scale as N^{-3} imply extended states while large IPR values which do not change much with system size denote localized states.

21

From Figs. (14,15) we make the following observations.

(i) From the $3D$ data it is clear the effect of localization is weaker than in $1D$ and $2D$. Both for $\Delta = 0.2$ and $\Delta = 0.8$ we find that there is transmission over almost the entire range of frequencies of the allowed normal modes. From the IPR plots we see that for $\Delta = 0.2$ most states are extended except for a small region in the band-edge. For $\Delta = 0.8$ the allowed modes form two bands and one finds significant transmission over almost the full range. At the band edges there are again localized states. It also appears that there are some large IPR states interspersed within the high frequency band. As in the $2D$ case and unlike the $1D$ case, the frequency range over which transmission takes place does not change with system size, only the overall magnitude of transmission coefficient changes.

(ii) The inset in Fig. (15) which plots $NT(\omega)$ throws light on the nature of the extended states. The high frequency band and a portion of the lower frequency band have the scaling $T(\omega) \sim N^{-1}$ and hence corresponds to diffusive states. In the low-frequency band the fraction of diffusive states seems to be increasing with system size. The lowest frequency states have a system-size independent $T(\omega)$ and are thus ballistic states and this region is expected to scale as $N^{-1/4}$. The ballistic nature of low-frequency states is also verified in Fig. (14) where we see that $T(\omega)$ for the binary-mass ordered and disordered lattices match for small ω [with a $T(\omega) \sim \omega^5$ dependence]. Finally as in the $2D$ case here too we find that there is a region between the ballistic and diffusive regimes where $T(\omega)$ has non-trivial scaling.

In Fig. (16) we show the system size dependence of the disorder averaged current density J for the two cases with weak disorder strength ($\Delta = 0.2$) and strong disorder strength ($\Delta = 0.8$). The results for cubic lattices of sizes up to $N = 32$ are from the numerical method while the results for larger sizes are from simulations. We find an exponent $\mu \approx 0.6$ at small disorder and $\mu \approx 0.75$ at large disorder strength. As in the $2D$ case here too we believe that at small disorder, the asymptotic system size limit will be reached at much larger system sizes and that the exponent obtained at large disorder strength is probably close to the true asymptotic value. The value ($\mu = 0.75$) does not agree with the prediction ($J \sim N^{-1}$) made from the heuristic arguments in Sec. (IV). The reason for the breakdown of the argument is probably due to the intermediate states between the ballistic and diffusive regime which must be super-diffusive.

The data point at $N = 128$ for the set with $\Delta = 0.2$ in Fig. (16) actually corresponds

to a lattice of dimensions $128 \times 48 \times 48$ and we believe that the current value is very close to the expected fully $3D$ value. To see this point, we have plotted in Fig. (17) results from simulations with $N \times N_2 \times N_2$ lattices with $N_2 \leq N$.

Finally, in Fig. (18) we show temperature profiles (for single disorder realizations) obtained from simulations for lattices of different sizes and with $\Delta = 0.2$. The jumps at the boundaries again indicate that the asymptotic system size limit has not been reached even at the largest size.

Free BC: In this case from the arguments in Sec. (IV) we expect ballistic states to contribute most significantly to the current density giving $J_{\text{ball}} \sim N^{-3/4}$. From the results for fixed BC the contribution of the non-ballistic extended states is expected to scale as $N^{-0.75}$. Hence the overall current should scale in the asymptotic limit as $J \sim N^{-0.75}$.

In Fig. (19) we plot the disorder averaged transmission coefficient for $\Delta = 0.8$ for different system sizes. The transmission function is very close to that for the fixed boundary case except in the frequency region corresponding to non-diffusive states. At $\omega \to 0$ we now expect, though it is hard to verify from the data, that $T(\omega) \sim \omega^2$ in contrast to $T(\omega) \sim \omega^4$ for fixed boundaries.

The system size dependence of the disorder averaged current J for two different values of Δ is shown in Fig. (16). We find that the current values are quite close to the fixed BC case and the exponent obtained at the largest system size studied for this case is $\mu \approx 0.7$. This value is close to the expected $\mu = 3/4$ for free BC and thus probably the same as for the case with fixed BC. Thus the dependence of the value of μ on boundary conditions probably does not exist in three dimensions.

2. *Disordered $3D$ lattice with a substrate potential*

For the pinned case, we again use both the numerical method and simulations for sizes up to $N = 32$. For $N = 64$ only simulation results are reported.

In Figs. (20,21) we plot the disorder averaged transmission coefficient for $\Delta = 0.2$ and $\Delta = 0.8$ with $k_o = 10.0$. The corresponding IPRs P^{-1} and scaled IPRs $N^3 P^{-1}$ are also shown.

From the IPR plots we notice that the spectrum of the $3D$ disordered pinned chain has a similar interesting structure as in the $2D$ case with two bands and a gap which is seen at

Dimension	Fixed BC		Free BC		Pinned	
	Analytical	Numerical	Analytical	Numerical	Analytical	Numerical
Two	$N^{-1}(\ln N)^{-1/2}$	$N^{-0.75\pm0.01}$	$N^{-2/3}$	$N^{-0.6\pm0.01}$	$\exp-bN$	$\exp-bN$
Three	N^{-1}	$N^{-0.75\pm0.01}$	$N^{-3/4}$	$N^{-0.7\pm0.01}$	N^{-1}	$N^{-1.0\pm0.01}$

TABLE I: The table summarizes the main results of the paper. The numerical (and simulation) results obtained in the paper are compared, in two and three dimensions, with the analytical predictions obtained from our heuristic arguments.

strong disorder. However unlike the $2D$ case where all states were localized, here the IPR data indicates that most states except those at the band edges are diffusive. We see localized states at the band edges and also there seem to be some localized states interspersed among the extended states within the bands. The insets in Figs. (20,21) show that there is a reasonable N^{-1} scaling of the transmission data in most of the transmitting region. This is clearer at the larger system sizes. Thus, unlike the unpinned case where low frequency extended states were ballistic or super-diffusive, here we find that there is no transmittance at small ($\omega \to 0$) frequencies and that all states are diffusive. One might expect that at very strong disorder, all states should become localized and then one should get a heat insulator. The parameter set corresponding to Fig. (21) corresponds to quite strong disorder and for this we still find a significant fraction of extended states. Note that in the electronic case one is typically interested in the character of states at or close to the Fermi level and so a metal-insulator transition is easy to observe. In the phonon case since all states contribute, this is more difficult to observe, and it is not clear if at all such a transition will occur.

From the above discussion we expect Fourier's law to be valid in the $3D$ pinned disordered lattice. The system size dependence of the disorder averaged current J for different disorder strengths is plotted in Fig. (22). For all the parameter sets the exponent obtained is close to $\mu = 1$ corresponding to a finite conductivity and validity of Fourier's law. The temperature profiles plotted in Fig. (23) have small boundary temperature jumps and indicate that the asymptotic size limit has already been reached.

VI. DISCUSSION

In summary we have studied heat conduction in isotopically disordered harmonic lattices with scalar displacements in two and three dimensions. The main question addressed is the system size dependence of the heat current, which is computed using Green's function based numerical methods as well as nonequilibrium simulations. We have tried to understand the size dependence by looking at the phonon transmission function $T(\omega)$ and examining the nature of transport in different frequency regimes. We also described a heuristic analytical calculation based on results from localization theory and kinetic theory and compared their predictions with our numerical and simulational results. This comparison is summarized in Table (I).

The most interesting findings of this work are:

(i) In both two and three dimensions for the unpinned lattice, we find power law divergence of the conductivity, with the exponent being dependent on boundary conditions in $2D$ and probably independent of boundary conditions in $3D$. Our study of the phonon transmission function suggests that extended states can be classified into three classes. The states for frequencies $\omega < N^{-1/(d+1)}$ are ballistic and their contribution to total current depends on boundary conditions. There is an intermediate range of frequencies for $\omega > N^{-1/(d+1)}$ and less than some upper cut off where the extended states appear to be *non-diffusive* and instead show anomalous scaling suggesting super-diffusive behaviour. The remaining extended modes are diffusive.

(ii) In two dimensions the pinned disordered lattice shows clear evidence of localization and we obtain a heat insulator with exponential dependence of current on system size.

(iii) Our result for the $3D$ pinned disordered lattice provides the first microscopic verification of Fourier's law in a three dimensional system. We have not been able to see a transition to insulating behaviour with increasing disorder.

––––––––––––––––––

[1] A. Dhar, Adv. Phys., **57**, 457 (2008).

[2] S. Lepri, R. Livi, and A. Politi, Phys. Rep. **377**, 1 (2003).

[3] F. Bonetto, J.L. Lebowitz, and L. Rey-Bellet, in *Mathematical Physics 2000*, edited by A. Fokas et. al. (Imperial College Press, London, 2000), p. 128.

[4] C. W. Chang *et al.* , Phys. Rev. Lett. **101**, 075903 (2008).

[5] T. Shimada, T. Murakami, S. Yukawa, K. Saito and N. Ito, J. Phys. Soc. Jpn. **69**, 3150 (2000).

[6] H. Shiba and N. Ito, J. Phys. Soc. Jpn. **77**, 054006 (2008).

[7] P. W. Anderson, Phys. Rev. **109**, 1492 (1958).

[8] N. F. Mott and W. D. Twose, Adv. Phys. **10**, 107 (1961); R. E. Borland, Proc. R. Soc. London, Ser. A **274**, 529 (1963).

[9] P. A. Lee and T. V. Ramakrishnan, Rev. Mod. Phys. **57**, 287 (1985).

[10] H. Matsuda and K. Ishii, Prog. Theor. Phys. Suppl. **45**, 56 (1970).

[11] R. J. Rubin and W. L. Greer, J. Math. Phys. **12**, 1686 (1971).

[12] A. Casher and J. L. Lebowitz, J. Math. Phys. **12**, 1701 (1971.)

[13] A. J. O'Connor and J. L. Lebowitz, J. Math. Phys. **15**, 692 (1974).

[14] A. Dhar, Phys. Rev. Lett. **86**, 5882 (2001).

[15] D. Roy and A. Dhar, Phys. Rev. E **78**, 051112 (2008).

[16] S. John, H. Sompolinsky, and M. J. Stephen, Phys. Rev. B **27**, 5592 (1983).

[17] H. Spohn, private communication.

[18] L. Yang, Phys. Rev. Lett. **88**, 094301 (2002).

[19] B. Hu, Bai-Qi Jin, L. Wang, and H. Yang, Phys. Rev. Lett. **90**, 119401 (2003).

[20] L. W. Lee and A. Dhar, Phys. Rev. Lett. **95**, 094302 (2005).

[21] C. W. Chang *et al.* , Phys. Rev. Lett. **97**, 085901 (2006).

[22] I. Savic, N. Mingo and D. A. Stewart, Phys. Rev. Lett. **101**, 165502 (2008).

[23] G. Stoltz, M. Lazzeri and F. Mauri, arXiv:0810.1830.

[24] A. Dhar and D. Roy, J. Stat. Phys. **125**, 801 (2006).

[25] L. G. C. Rego and G. Kirczenow, Phys. Rev. Lett. **81**, 232 (1998).

[26] M. P. Blencowe, Phys. Rev. B **59**, 4992 (1999).

[27] T. Yamamoto and K. Watanabe, Phys. Rev. Lett. **96**, 255503 (2006).

[28] J. S. Wang, J. Wang and N. Zeng, Phys. Rev. B **74**, 033408 (2006).

[29] A. MacKinnon and B. Kramer, Z. Phys. B - condns. Matt. **53**, 1 (1983).

[30] J. Hori, *S*pectral properties of disordered chains and lattices, (Pergamon Press, Oxford, 1968).
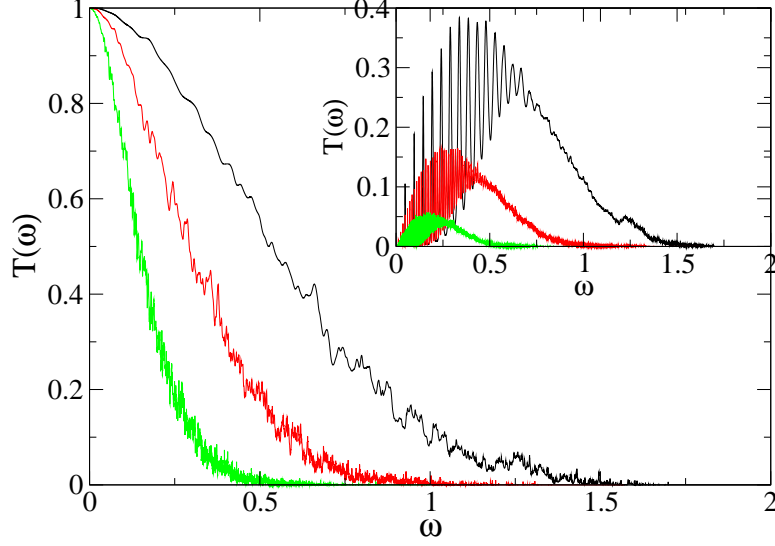
FIG. 1: (color online) $1D$ unpinned case with both free and fixed (INSET) boundary conditions: plot of the disorder averaged transmission $T(\omega)$ versus ω for $\Delta = 0.4$. The various curves (from top to bottom) correspond to lattices of sizes $N = 64, 256, 1024$ respectively.

[31] M.P. Allen and D.L. Tildesley, *Computer Simulation of Liquids* (Clarendon Press, Oxford, 1987).

[32] A. Dhar and J.L. Lebowitz, Phys. Rev. Lett. **100**, 134301 (2008).

[33] A. Kundu, A. Chaudhuri and A. Dhar, to be published.
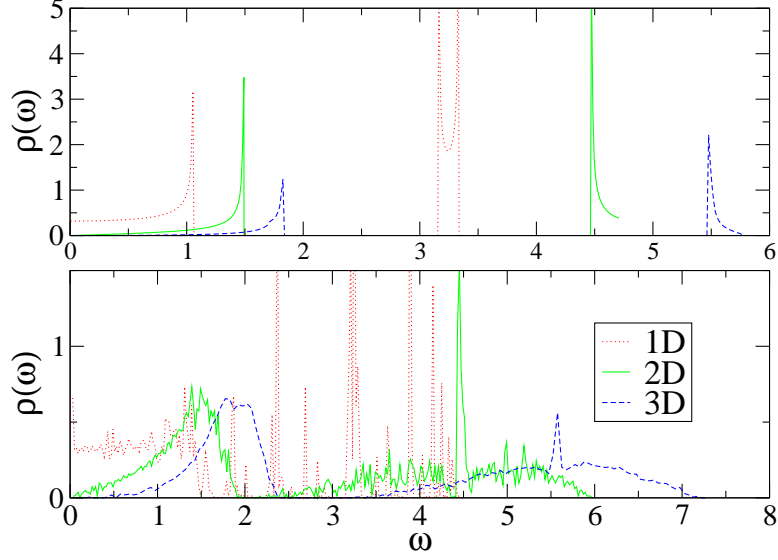
FIG. 2: (color online) Density of states versus ω.

TOP: Density of states obtained numerically for ordered binary mass lattices in $1D, 2D$ and $3D$.

BOTTOM: Density of states obtained numerically from the eigenvalues of single binary mass disorder realizations in $1D, 2D$ and $3D$ for lattice sizes $N = 4096, 64, 16$ respectively. Note that the low frequency behaviour is unaffected by disorder and one has ω^{d-1} as $\omega \to 0$. In all cases we have $\Delta = 0.8$ and $k = 1$.
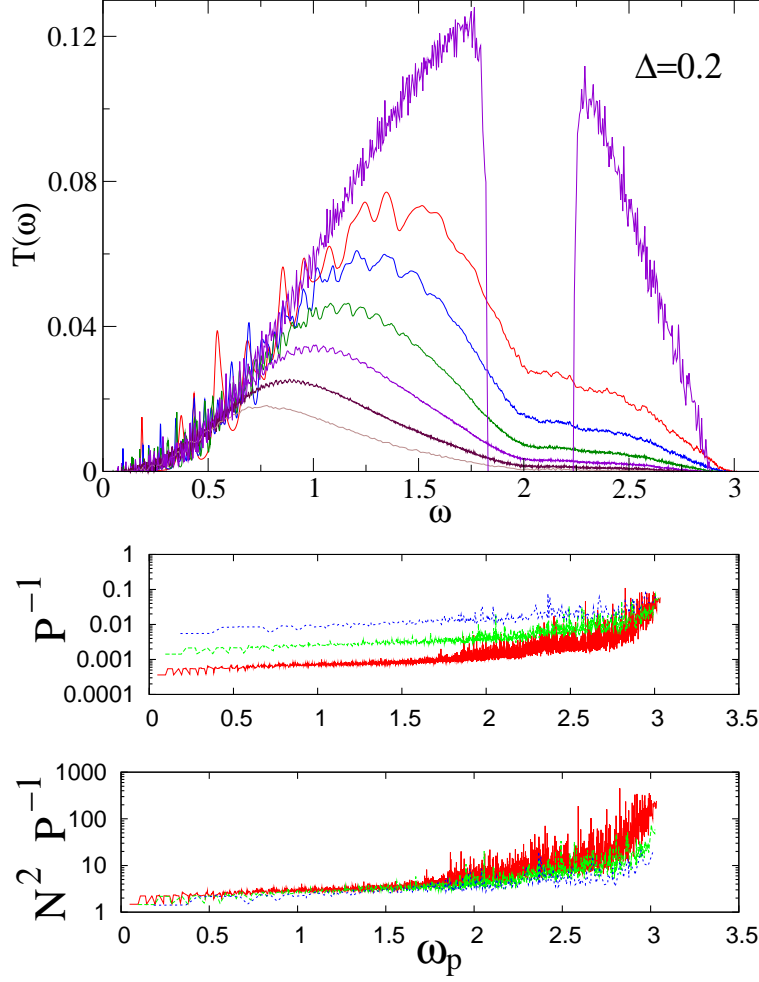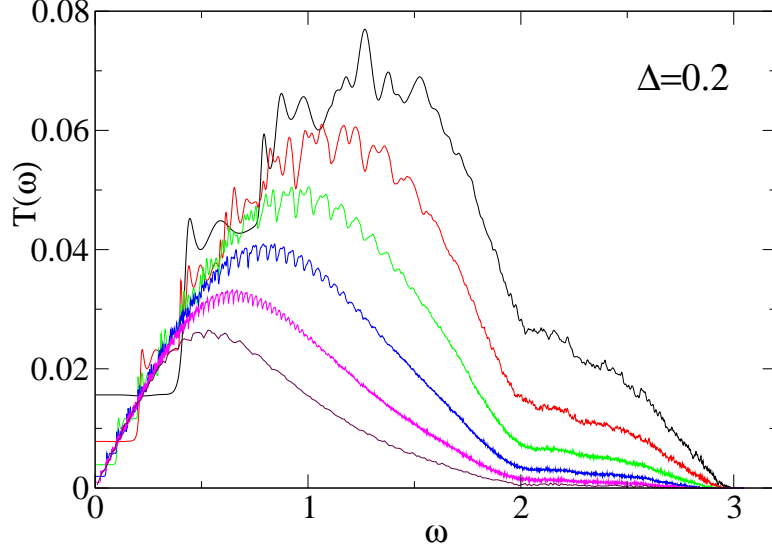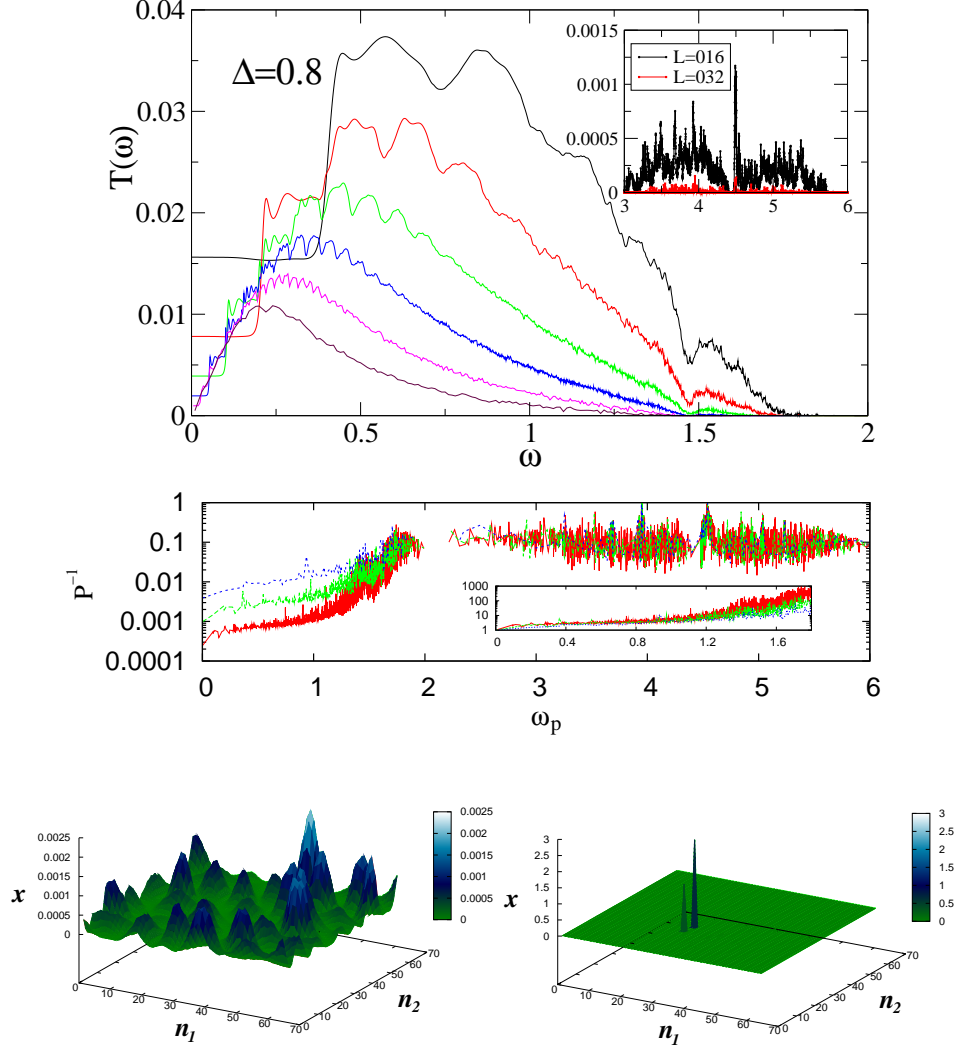
FIG. 3: (color online) 2D unpinned case with fixed BC for $\Delta = 0.2$

TOP: Plot of the disorder averaged transmission $T(\omega)$ versus ω. The upper-most curve corresponds to a binary-mass ordered lattice with $N = 128$ while the remaining curves (from top to bottom) correspond to square lattices with $N = 16, 32, 64, 128, 256, 512$ respectively.

BOTTOM: Plot shows the IPR (P^{-1}) and scaled IPR (N^2P^{-1}) as a function of normal mode-frequency ω_p. The curves are for $N = 16$ (blue), 32 (green) and 64 (red).
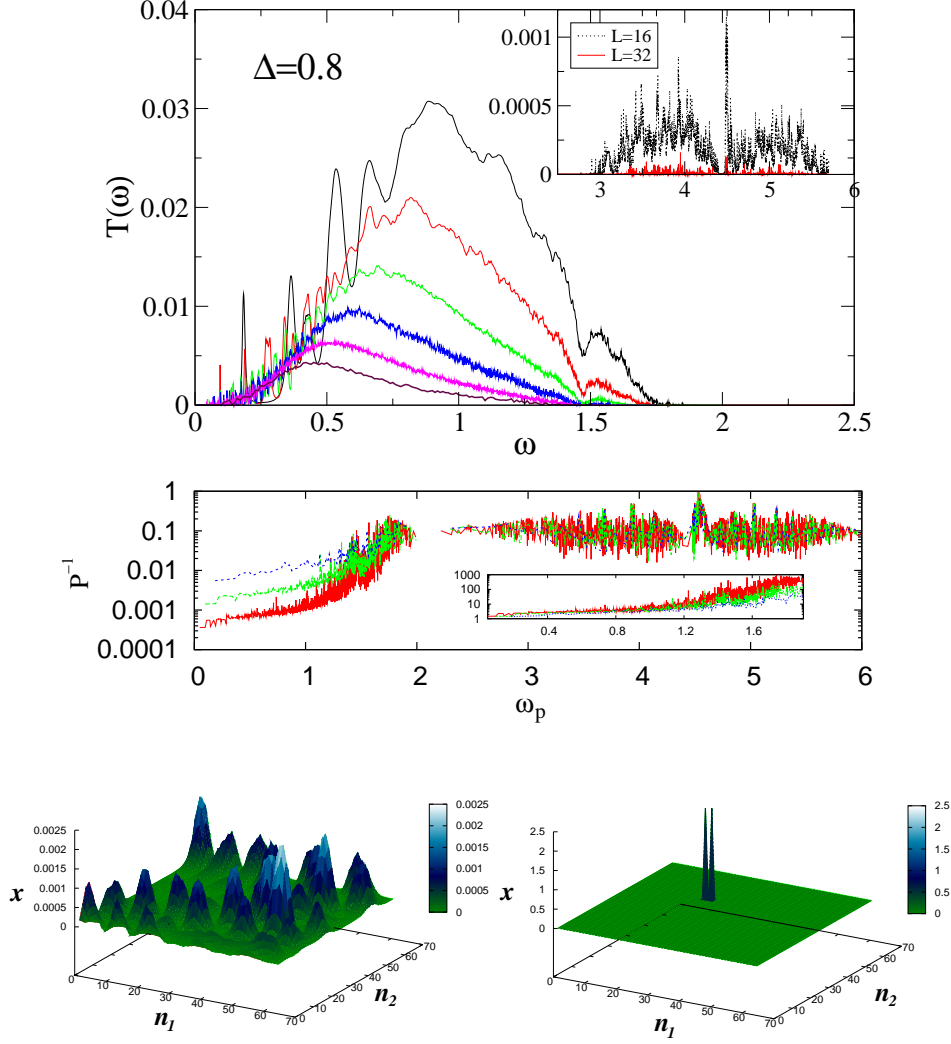
FIG. 4: (color online) $2D$ unpinned case with fixed BC for $\Delta = 0.8$

TOP: Plot of the disorder averaged transmission $T(\omega)$ versus ω. The various curves (from top to bottom) correspond to square lattices with $N = 16, 32, 64, 128, 256, 512$ respectively. We see that even though the allowed normal modes occur over a large frequency band $\approx (0 - 6)$, transmission takes place in a small band $\approx (0 - 2)$ and, as can be seen in the inset, is negligible elsewhere.

BOTTOM: Plot shows the IPR (P^{-1}) as a function of normal mode-frequency ω_p for the $2D$ lattice with $\Delta = 0.8$. The curves are for $N = 16$ (blue), 32 (green) and 64 (red). The inset plots $N^2 P^{-1}$ and the collapse at low frequencies shows that these modes are extended. Also shown are two typical normal modes for one small (left) and one large value of P^{-1} for $N = 64$.
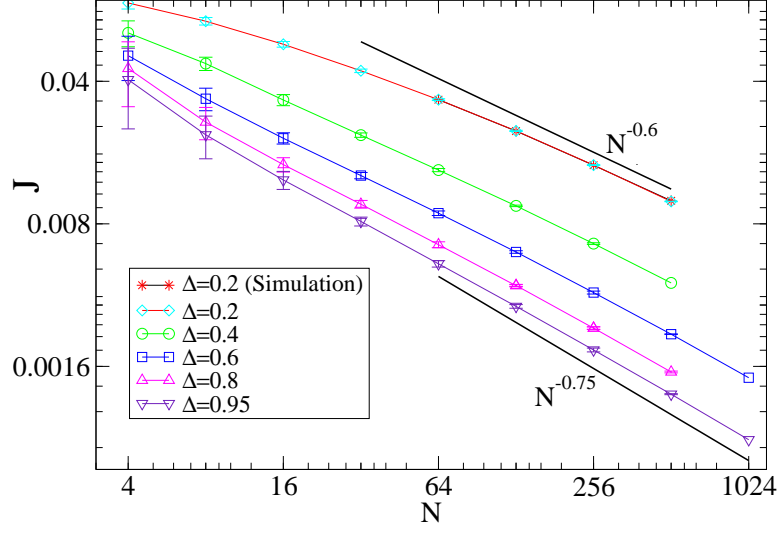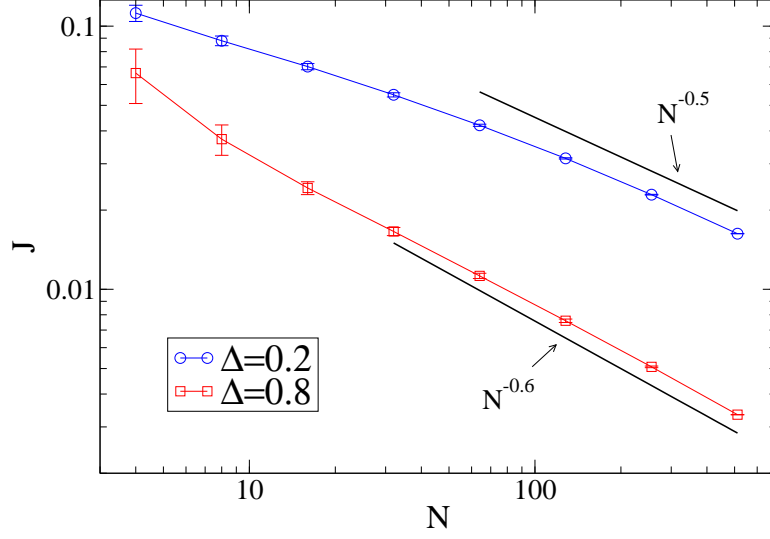
FIG. 5: (color online) $2D$ unpinned lattice with fixed BC

Plot of disorder-averaged current J versus system size for different values of Δ. The error-bars show the actual standard deviations from sample-to-sample fluctuations. Numerical errors are much smaller. For $\Delta = 0.2$, simulation data is also plotted.
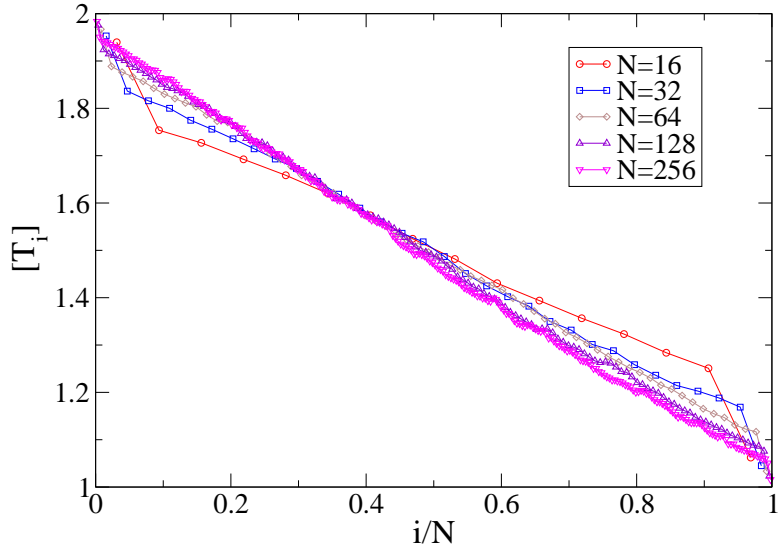

FIG. 6: (color online) $2D$ unpinned case with fixed BC for $\Delta = 0.2$

Plot of disorder-averaged temperature profile $[T_i]$ for different system sizes obtained from simulations.

FIG. 7: (color online) $2D$ unpinned case with free BC for $\Delta = 0.2$.

Plot of the disorder averaged transmission $T(\omega)$ versus ω for. The curves (from top to bottom) are for $N = 16, 32, 64, 128, 256, 512$ respectively. Note the linear form at small ω.

FIG. 8: (color online) 2D unpinned case with free BC for $\Delta = 0.8$.

TOP: Plot of the disorder averaged transmission $T(\omega)$ versus ω. The various curves (from top to bottom) correspond to square lattices with $N = 16, 32, 64, 128, 256, 512$ respectively. We see that transmission takes place in a small band $\approx (0-2)$ of the full range $\approx (0-6)$ of normal modes and as can be seen in the inset is negligible elsewhere.

BOTTOM: Plot shows the IPR (P^{-1}) as a function of normal mode-frequency ω_p. The curves are for $N = 16$ (blue), 32 (green) and 64 (red). In the inset we plot $N^2 P^{-1}$ and the collapse at low frequencies shows that low frequency modes are extended. Also shown are two typical normal modes for one small (left) and one large value of P^{-1} for $N = 64$.
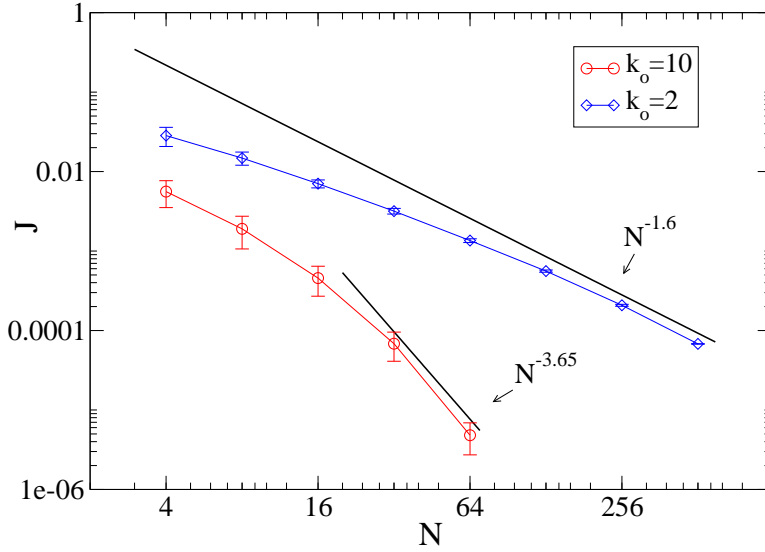
FIG. 9: (color online) $2D$ unpinned case with free BC

Plot of disorder-averaged current J versus system size for two different values of Δ. The error-bars show standard devations due to sample-to-sample fluctuations. Numerical errors are much smaller.
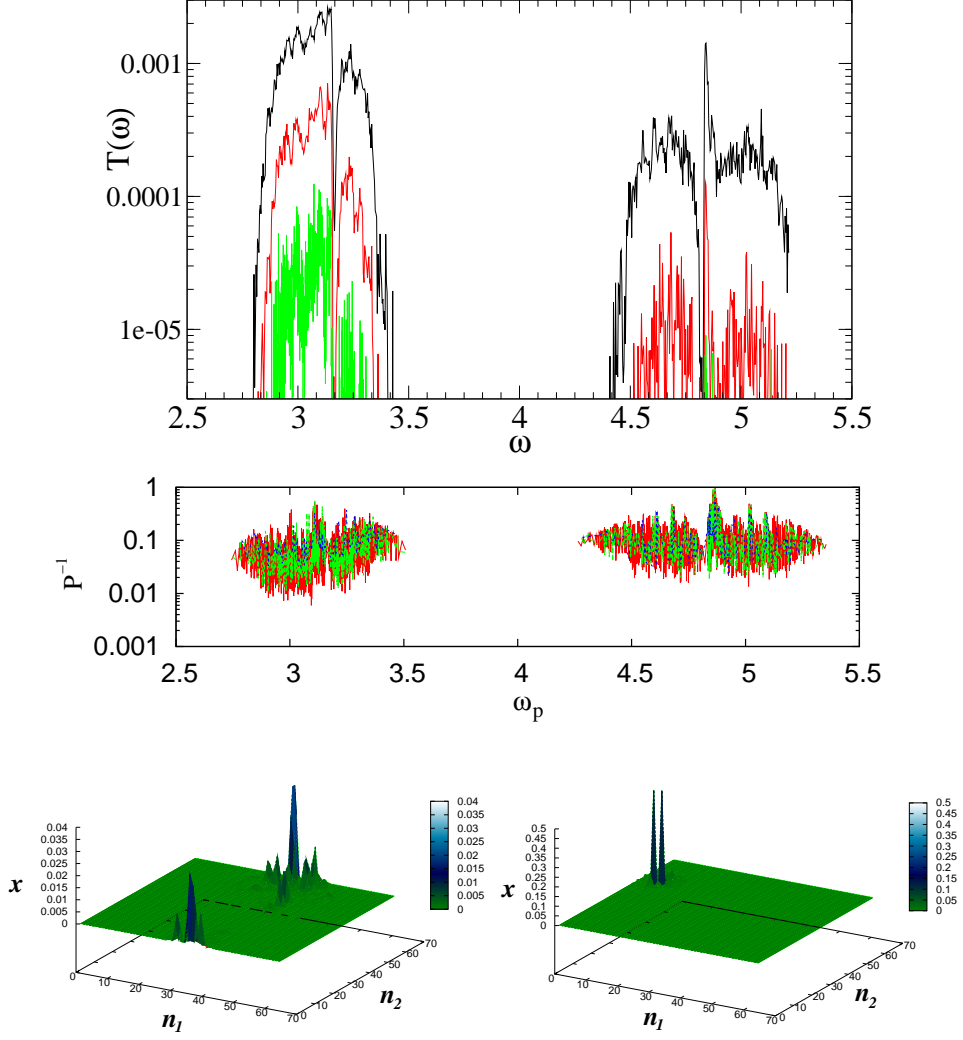
FIG. 10: (color online) 2D pinned case for $\Delta = 0.4$ and $k_o = 10.0$.

TOP: Plot of the disorder averaged transmission $T(\omega)$ versus ω. The various curves (from top to bottom) correspond to lattices with $N = 16, 32, 64$ respectively. Here we choose $\gamma = \sqrt{10}$.

BOTTOM: Plot of the IPR (P^{-1}) as a function of normal mode-frequency ω_p. The curves are for $N = 16$ (blue), 32 (green) and 64 (red). Also shown are two typical normal modes for one small (left) and one large value of P^{-1} for $N = 64$.
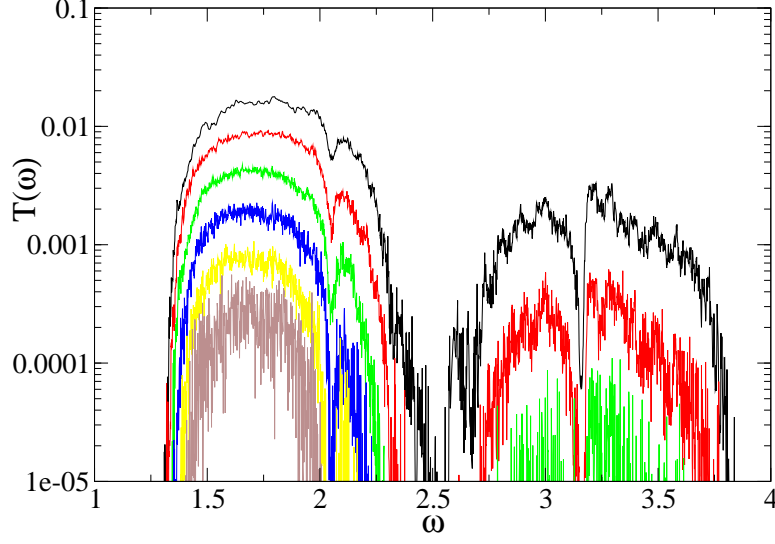
FIG. 11: (color online) $2D$ pinned case for $\Delta = 0.4$ and $k_o = 2.0$.

Plot of the disorder averaged transmission $T(\omega)$ versus ω . The various curves (from top to bottom) are for $N = 16, 32, 64, 128, 256, 512$ respectively. Here we choose $\gamma = \sqrt{2}$.

FIG. 12: (color online) $2D$ pinned case for $\Delta = 0.4$

Plot of disorder-averaged current J versus system size for two different values of k_o. Error bars show standard deviation due to disorder and numerical errors are much smaller. Note that the standard deviation do not decrease with system size for higher k_o.
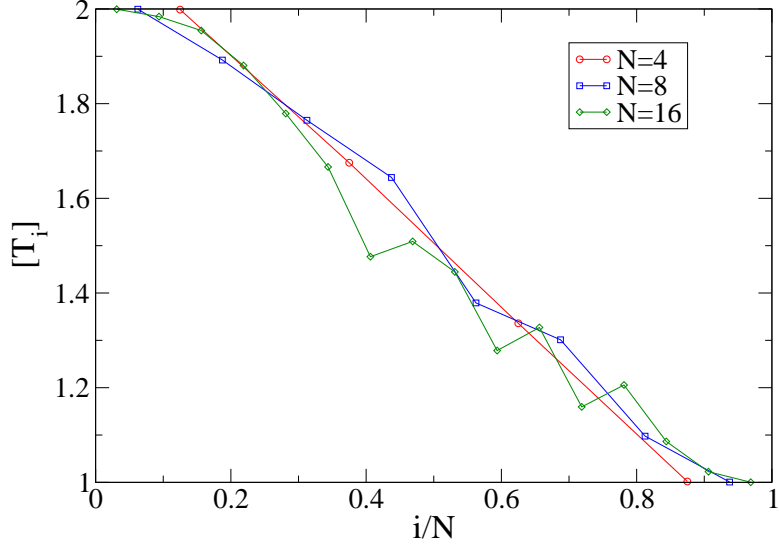
FIG. 13: (color online) $2D$ pinned case for $\Delta = 0.4$ and $k_o = 10.0$

Plot of disorder-averaged temperature profile $[T_i]$ for different system sizes. The plots are from simulations and here we choose $\gamma = \sqrt{10}$.
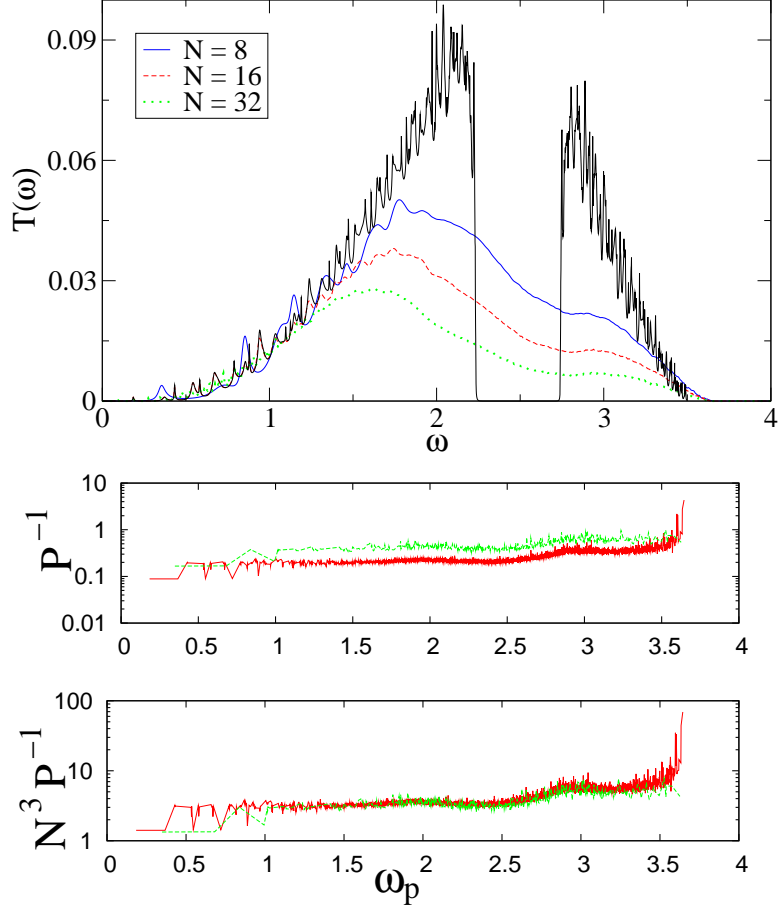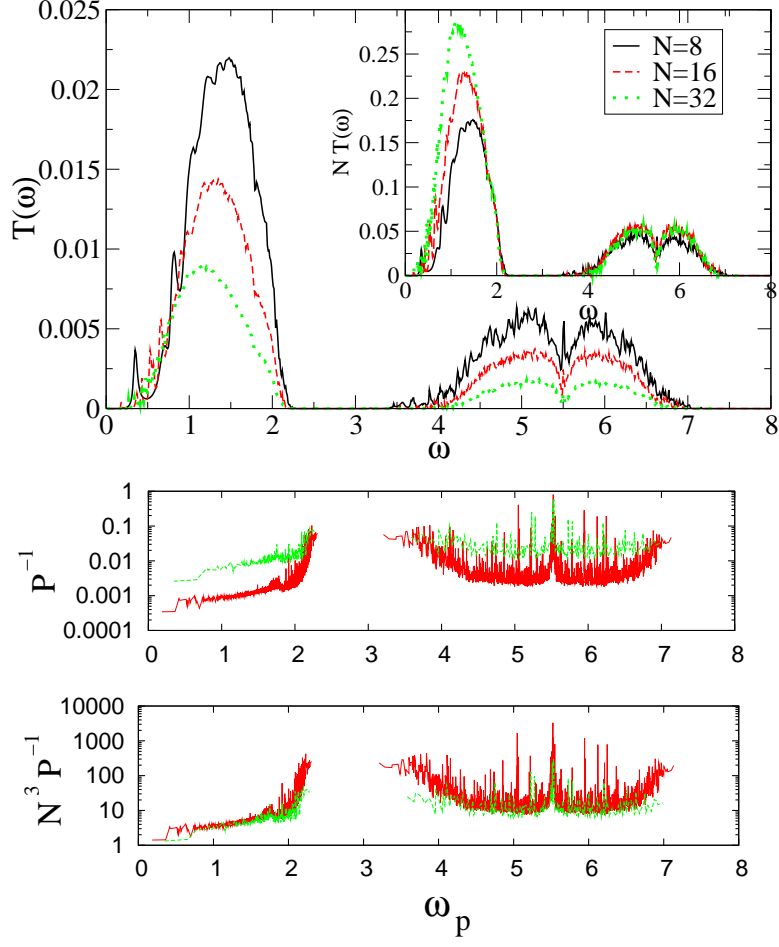
FIG. 14: (color online) $3D$ unpinned case with fixed BC for $\Delta = 0.2$.

TOP: Plot of the disorder averaged transmission $T(\omega)$ versus ω. The uppermost curve is the transmission curve for the binary mass ordered lattice for $N = 16$.

BOTTOM: Plot of IPR (P^{-1}) and scaled IPR ($N^3 P^{-1}$) as a function of normal mode-frequency ω_p for a fixed disorder-realization. The curves are for $N = 8$ (green) and 16 (red).
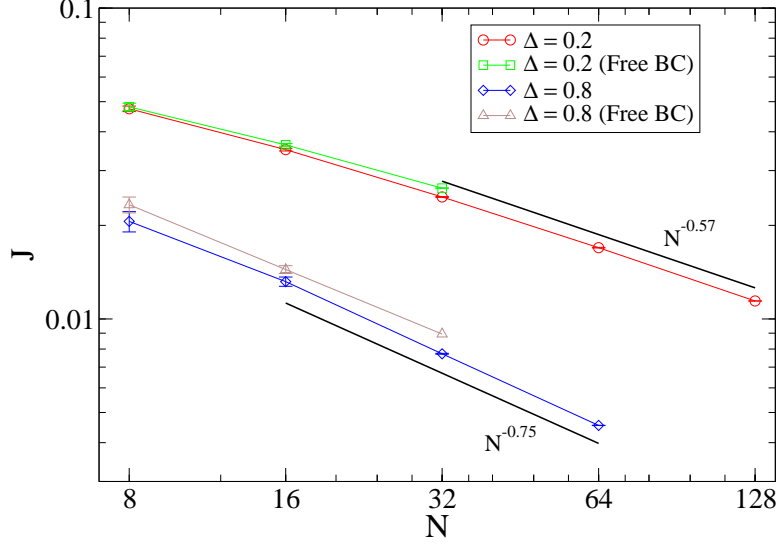
FIG. 15: (color online) $3D$ unpinned case with fixed BC for $\Delta = 0.8$.

TOP: Plot of the disorder averaged transmission $T(\omega)$ versus ω. The inset shows the same data multiplied by a factor of N.

BOTTOM: Plot of the IPR (P^{-1}) and scaled IPR $(N^3 P^{-1})$ as a function of normal mode-frequency ω_p for a fixed disorder-realization. The curves are for $N = 8$ (green) and 16 (red).

FIG. 16: (color online) $3D$ unpinned case with fixed BC

Plot of disorder-averaged current J versus system size for two different values of Δ. The data for $\Delta = 0.2$ is from simulations. The error-bars show standard deviations due to disorder and numerical errors are smaller.
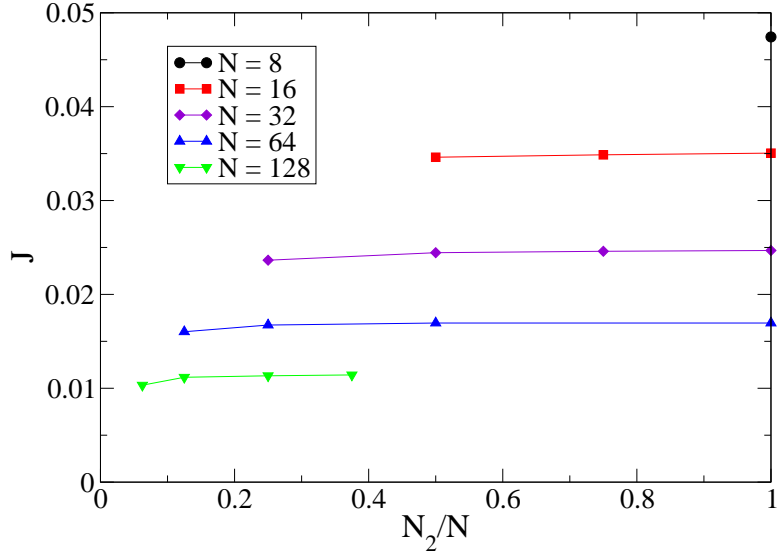
FIG. 17: (color online) $3D$ unpinned case with fixed BC for $\Delta = 0.2$

Plot of disorder-averaged current density J (with the definition $J = I/N_2^2$) versus N_2/N for different fixed values of N. We see that the 3D limiting value is reached at quite small values of N_2/N.
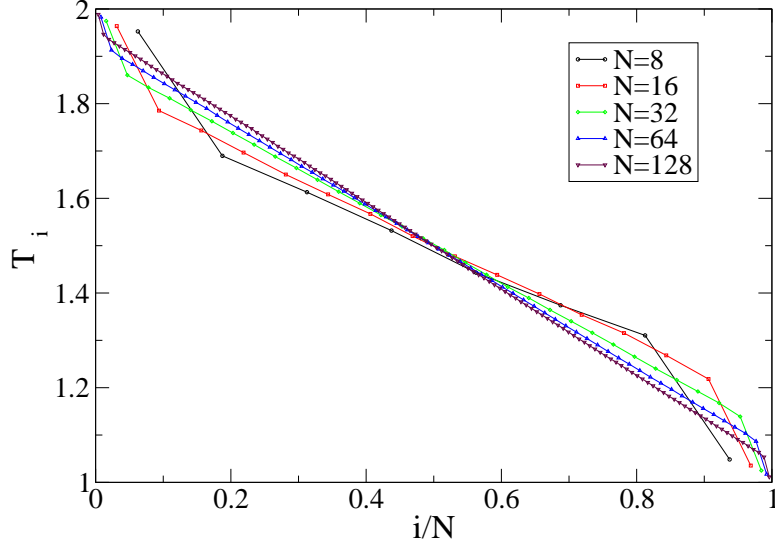
FIG. 18: (color online) $3D$ unpinned case with fixed BC for $\Delta = 0.2$

Plot of temperature profile T_i in a single disorder realization for different system sizes. The plots are from simulations..
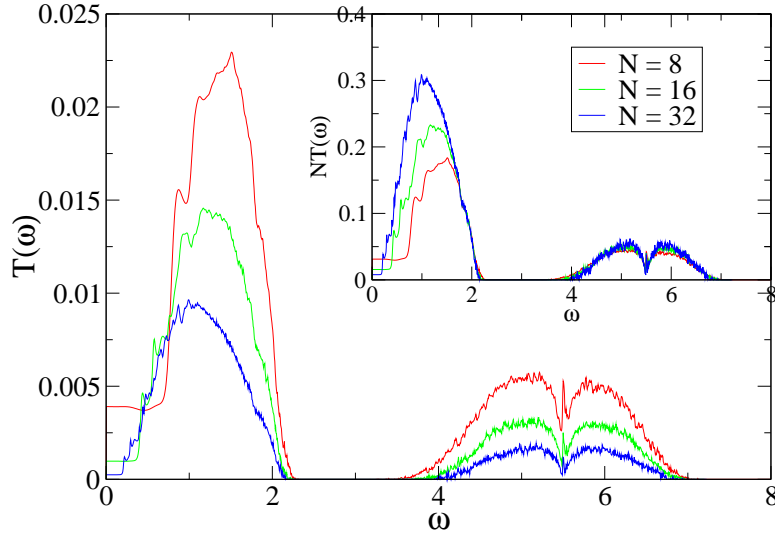

FIG. 19: (color online) $3D$ unpinned case with free BC for $\Delta = 0.8$.

TOP: Plot of the disorder averaged transmission $T(\omega)$ versus ω. The inset shows the same data multiplied by a factor of N.
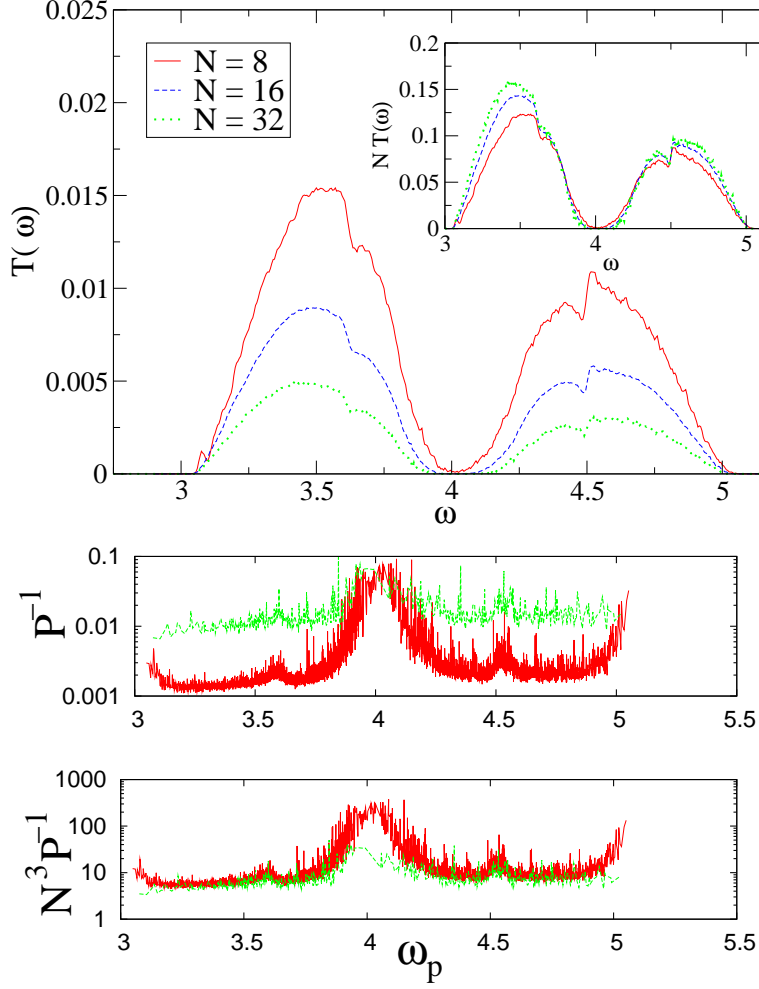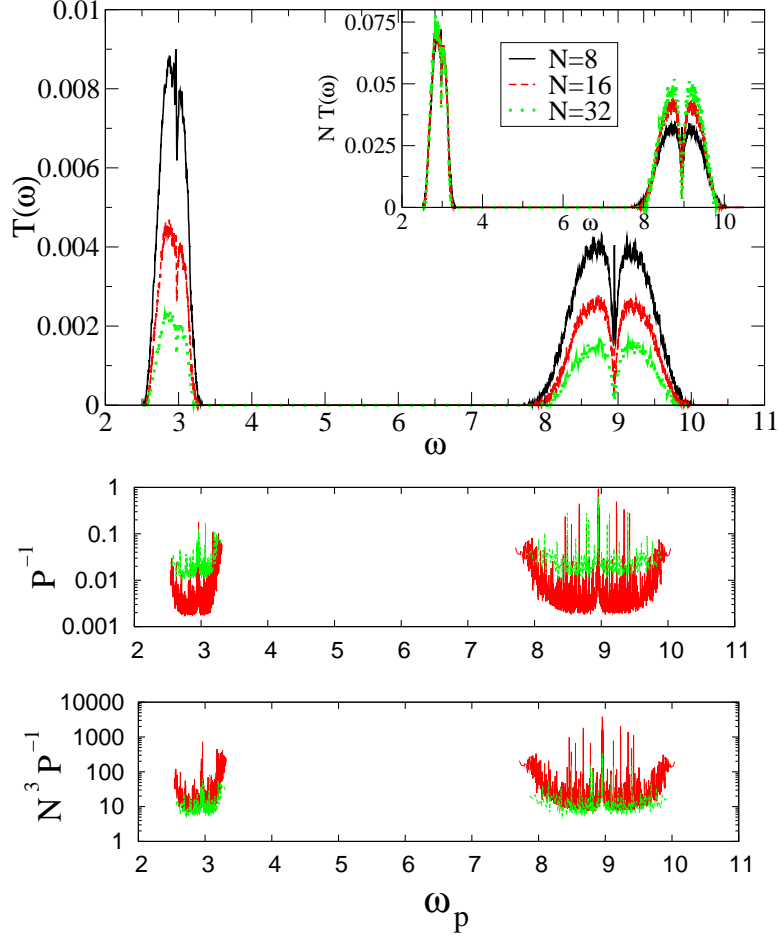
FIG. 20: (color online) $3D$ pinned case for $\Delta = 0.2$ and $k_o = 10.0$.

TOP: Plot of the disorder averaged transmission $T(\omega)$ versus ω.

BOTTOM: Plot of the IPR (P^{-1}) and scaled IPR ($N^3 P^{-1}$) as a function of normal mode-frequency ω_p. The curves are for $N = 8$ (green) and 16 (red).

FIG. 21: (color online) 3D pinned case for $\Delta = 0.8$ and $k_o = 10.0$.

TOP: Plot of the disorder averaged transmission $T(\omega)$ versus ω.

BOTTOM: Plot of the IPR (P^{-1}) scaled IPR $(N^3 P^{-1})$ as a function of normal mode-frequency ω_p. The curves are for $N = 8$ (green) and 16 (red).
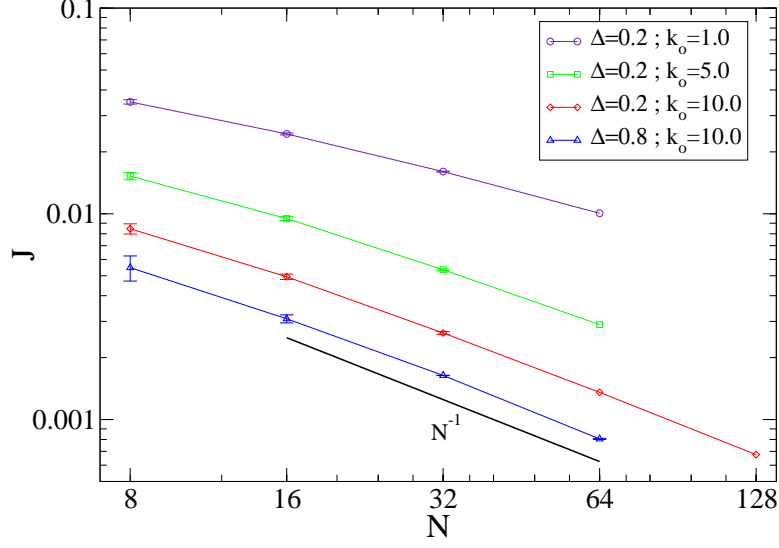
FIG. 22: (color online) $3D$ pinned case

Plot of disorder-averaged current J versus system size for different values of k_o and Δ. The data sets for $\Delta = 0.2$ for different values of k_o are from simulations while the data for $\Delta = 0.8$ is from numerics.
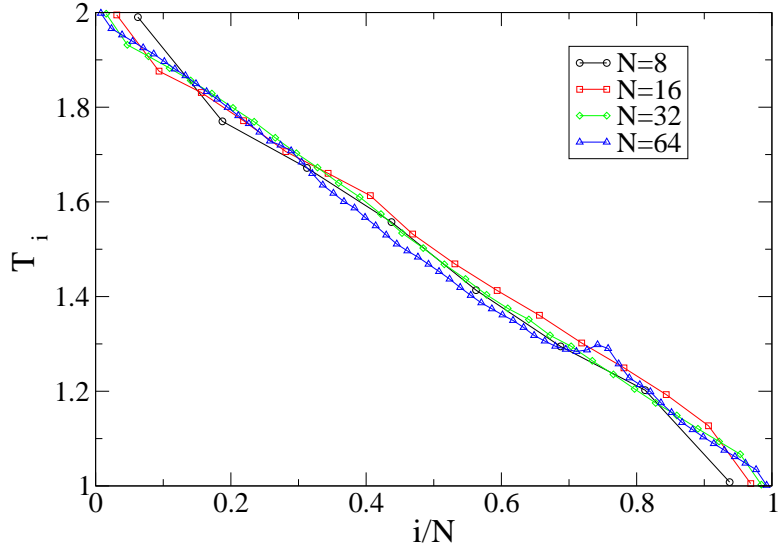

FIG. 23: (color online) $3D$ pinned case for $\Delta = 0.2$ and $k_o = 10.0$.

Plot of temperature profile T_i in a single disorder realization for different system sizes. The plots are from simulations.